Ore Geology Reviews 65 (2015) 545–563

Contents lists available at ScienceDirect

Ore Geology Reviews

journal homepage: www.elsevier.com/locate/oregeorev

# Alteration-mineralization, and radiometric ages of the source pluton at the Sangan iron skarn deposit, northeastern Iran

A. Golmohammadi [a], M.H. Karimpour [b], A. Malekzadeh Shafaroudi [b,*], S.A. Mazaheri [a]

[a] Ferdowsi University of Mashhad, P.O. Box 91775-1436, Mashhad, Iran
[b] Research Center for Ore Deposit of Eastern Iran, Ferdowsi University of Mashhad, P.O. Box 91775-1436, Mashhad, Iran

ARTICLE INFO

*Article history:*
Received 23 October 2012
Received in revised form 19 June 2014
Accepted 7 July 2014
Available online 12 July 2014

*Keywords:*
Sangan iron skarn
Ca-skarn
Mg-skarn
Syenite porphyry
KKB-VPMB
NE Iran

ABSTRACT

The world-class Sangan iron skarn deposit with a proven reserve of > 1000 Mt iron ore @ 53% Fe, is located in the Khaf-Kashmar-Bardaskan Volcano-Plutonic Metallogenic Belt (KKB-VPMB) of northeastern Iran along the E–W trending regional Doruneh Fault, north of the Lut Block. Skarn mineralization occurs at the contact of the 39.1 ± 0.6 Ma to 38.3 ± 0.5 Ma Middle Eocene syenite to syenogranite porphyry source pluton with Cretaceous carbonate rocks. The source pluton is part of an I-type, calcalkaline granitoid series with potassium to shoshonitic affinity, metaluminous to slightly peraluminous character. The granitoids are enriched in LILE (Cs, Rb, Ba, K, Th, and U) and LREE (La and Ce), are depleted in HFSE (Nb, Y, Ta, and Ti), HREE (Yb and Lu) and Eu, which together with the low Sr (96 to 362 ppm) and $(La/Yb)_N$ contents suggest a metasomatized, slab-derived mantel source within the Cenozoic volcanoplutonic continental arc of northeaster Iran. The location of the skarn orebodies is controlled by the regional E–W Doruneh Fault structure, and the spatial distribution and the two, calcic and magnesian, skarns is controlled by the composition of the carbonate protolith that consists of limestone in the west and dolomite in the east. The chemistry of the skarn minerals reflects the composition of the protoliths. The western skarn is dominated by ca-rich calcsilicates that consist of prograde Ca-rich garnet ($Adr_{50-97}Grs_{0-45}Sps\text{-}Alm_{2-7}$), Ca–Fe-rich pyroxene ($Hd_{75.6}Di_{20}$ $Jo_{4.5}$), K–Cl–F-bearing Fe–Ca-rich amphibole ferrohastingsite ($Fe_{4.4}Ca_2Mg_{0.5}K_{0.4}Na_{0.3}$)($Si_{6.5}Al_{1.8}O_{22}$)(Cl, F, OH)$_2$ in endoskarns, and retrograde ferroactinolite ($Fe_{4.2}Ca_2MgMn_{0.04}Na_{0.1}K_{0.06}$)($Si_{7.8}Al_{0.2}O_{22}$)(F, Cl, OH)$_2$ and Fe-rich chlorite ripidolite ($Fe_{4.3}Mg_{1.1}Ca_{0.06}Mn_{0.01}$)($Al_{2.8}Si_3O_{10}$)$(OH)_8$ in the exoskarns. Wollasonite, plagioclase, and K-feldspar have been additionally formed together with ferrohastingsite in the endoskarns. The eastern magnesian skarn is typically phlogopite-rich ($K_{0.9}Mg_{2.7}Fe_{0.2}Na_{0.02}$)($Si_{2.9}Al_{1.2}O_{10}$)(OH, F)$_2$, and consists of prograde forsterite ($Fo_{97.0}Fa_{2.7}$), diopsidic pyroxene ($Hd_{0.2}Di_{0.88}$), and retrograde Mg-rich actinolite, Mg-rich chlorite clinochlore ($Mg_{4.5}Fe_{0.1}K_{0.05}$)($Al_{1.8}Si_{2.7}O_{10}$)$(OH)_8$, serpentine and talc. Iron mineralization overprints the calcsilicate skarns in both the western and the eastern skarns and is magnesian in the eastern orebodies (3.65 wt.% MgO). The iron ore consists of a number of high grade, replacement, and magnetite orebodies with minor amounts of pyrrhotite, chalcopyrite, and pyrite indicating a large scale metasomatic transfer of iron bearing fluids during Middle Eocene magmatic activity at the KKB-VPMB.



## 1. Introduction

The Sangan iron skarn deposit at the Khorassan Department in northeastern Iran is located at the eastern edge of the Khaf-Kashmar-Bardaskan Volcano-Plutonic-Metallogenic Belt—KKB-VPMB (Fig. 1) Having a proven reserve of over 1000 Mt iron ore @ 53 % Fe, Sangan represents a worldclass iron skarn deposit. The skarns and the iron orebodies, defined by surface mapping and diamond drilling, extend over an E–W trending zone of around 8 km, and occur at depths down to 600 m below the surface. The iron ore consists of seven orebodies or anomalies defined in the mine as (Á), (A), (B), (C-South or Cs), (C-North or Cn), Baghak, and Dardvay from the west to the east. Historic records of iron ore at Sangan are known since 600 years (Mostowfi Ghazvini, 1339), although significant mining activity only started after 1975. Extensive modern exploration began in 1983 by the National Iranian Steel Company (NISCO) and continued by Madankav and Kavoshgaran companies in 2004 that resulted in 240,000 m of bore cores and the definition of an iron ore reserve of more than 1000 Mt grading @ 53% Fe.

Previous studies were mainly limited to the alteration and mineralization characteristics of selected parts of the Sangan deposit (Boomeri, 1998; Karimpour, 1999; Karimpour and Malekzadeh Shafaroudi, 2006, 2008; Mazloomi et al., 2009; Yousefi et al., 2009). A number of questions such as the petrochemistry of the different intrusions, their relationship with the iron skarn ore and their relative ages, and the nature of the magmatism were still unclear. The present paper is the result of the PhD study of the first author and is based on extensive field works and the recognition of different intrusive bodies, their radiometric age determination and

* Corresponding author.

http://dx.doi.org/10.1016/j.oregeorev.2014.07.005
0169-1368/

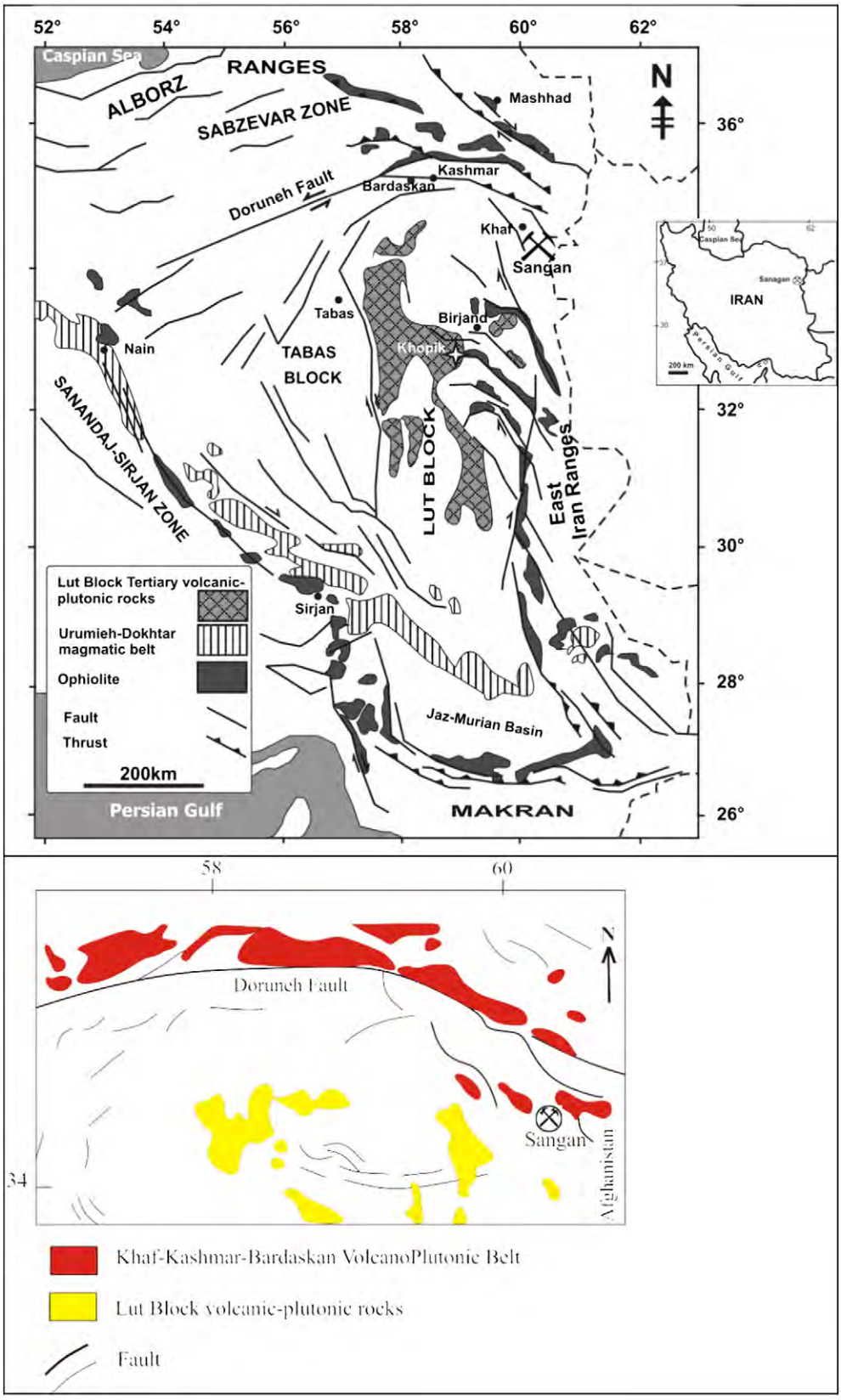


**Fig. 1.** Simplified structural map of eastern Iran showing the location of the Sangan deposit at the eastern edge of Doruneh Fault (modified from Malekzadeh et al., this volume), the Khaf-Kashmar-Bardaskan Volcanoplutonic Belt, and the southerly Cenozoic volcanoplutonic rocks of the Lut Block.

relationships with skarn mineralization, as well as the mineralogy and mineral chemistry of the skarns. An outcome of this study was the recognition of two distinct zones of calcic and magnesian skarns controlled by the composition of the metasomatized prototype carbonate host rocks. The results have been summarized in a schematic model for the skarn mineralization at Sangan.

## 2. Analytic methods

Following repeated field works with sampling and detailed core logging and petrographic studies of more than five hundred samples from different skarns and orebodies in the west and in the east and on the magmatic rocks, representative samples were selected for the following analyses. Ten samples from the intrusions in the area of (Á) orebody were analyzed for bulk rock chemistry. Major elements were determined by wave-length dispersive X-ray fluorescence spectrometer using fused disks, and by a Phillips PW 1480 XRF spectrometer at the Ferdowsi University of Mashhad, Iran. A set of international and Iranian rock standards including MRG-1, MG-4, JG-2, JR-1, SY-2, SY-3, JSL-1, MK-1, NIM-S, and NCS-307, were used for calibration. Trace elements and rare earth element analyses were done by inductively coupled plasma-mass spectrometry (ICP-MS) at the ACME Analytical Laboratories Ltd., Canada.

The mineral chemistry of the magnetite ore from the western and eastern orebodies, and a limited number of calksilicate skarn minerals was determined by electron microprobe at the University of Tasmania, Australia. The analyses were performed on a Cameca SX50 equipped with five asynchronous wavelength dispersive spectrometers and PGT PRIMS2000 energy dispersive X-ray detector. The analytic conditions were 15 kV acceleration voltage and 20 nA sample current for magnetite and garnet, 15 nA for amphibole and pyroxene, and 10 nA for chlorite and phlogopite. Counting times were 30 s on peak for all elements, yielding calculated minimum levels of detection (at $3\sigma$ above mean background) of $\leq$0.02 wt.% of the oxide for all components. Natural minerals and synthetic compounds were used as standards.

Two rock samples were selected for U–Pb zircon age dating from the source intrusions north of the Anomaly (Á), one from the biotite hornblende quartz alkali syenite porphyry (sample Stp-34), and another from the hornblende biotite syenogranite porphyry (sample Saf-170). Around 70 zircon grains were isolated from each rock sample by using standard mineral separation techniques at Ferdowsi University of Mashhad. U–Pb isotope data were collected using a New Wave 193 nm ArF laser ablation system coupled to a Nu Plasma HR inductively coupled plasma-mass spectrometer (ICP-MS) at the Arizona Laserchron Center using methods described by Gehrels et al. (2008).

Twenty-one magnetite ore samples from different orebodies of the Sangan mine were analyzed at the Sangan laboratories. The Fe content was determined by wet chemistry method using an international standard sample (No. 502-319) for calibration. The sulfur concentration was analyzed by wave-length dispersive X-ray fluorescence spectrometry on a LECO CS-230 XRF spectrometer, and the phosphorous on a Shimadzu UV-160A spectrometer using a MBH standard sample. Trace and rare earth elements were determined by inductively coupled plasma-mass spectrometry (ICP-MS) in the ACME Laboratory, Canada for fifteen ore samples.

## 3. Regional geology and tectonic setting

The Sangan iron skarn deposit is located at the eastern edge of the Khaf-Kashmar-Bardaskan Volcano-Plutonic and Metallogenic Belt (KKB-VPMB) of northeastern Iran. The KKB-VPMB is an arcute, W–E to NW–SE trending, Cenozoic volcano-plutonic arc of 400 km extension and 50 km width along the major Doruneh Fault that separates the KKB-VPMB from the southerly Lut Block (Fig. 1). Numerous iron, copper, and gold deposits and occurrences (e.g., Kuh-e-Zar, Shahrak, Tannurjeh, Sanagn) indicate that the KKB-VPMB is a metallogenic belt of a great economic potential (Karimpour, 2004; Mazloomi et al., 2009; Yousefi et al., 2009). The actual regional tectonomorphology results from the final Alpidic orogenesis, whereas the main lineaments and the general strike of the mountain ranges reflect reactivation of the earlier Assyntic orogenic structures (Eftekharnejad, 1981). The two blocks of Sabzevar in the north and Lut in the south of the Doruneh Fault show dextral and sinstral movements in different periods with the dextral movement being the last movements (Aghanabati, 2004). The structural features of the region such as faults and foldings, as well as the strike of the formations follow the NW–SE to E–W direction of the major Doruneh Fault. A series of NW–SE striking faults (N150) with

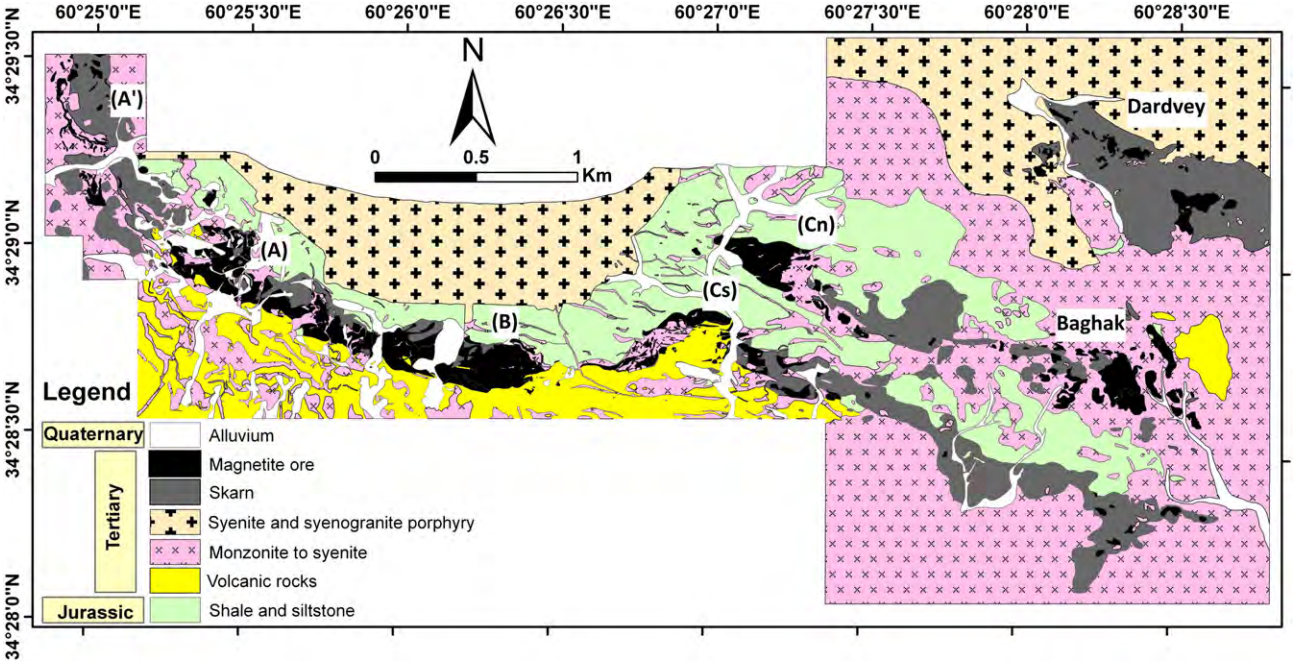


**Fig. 2.** Geological map of the Sangan deposit showing the source syenite-syenogranite porphyry and the slightly older barren monzonite to syenite, the Jurassic succession, and the Cretaceous carbonate rocks that are replaced by the calcsilicate-magnetite ore skarns in anomalies (Á), (A), (B), C-south (Cs), C-north (Cn), Baghak, and Dardvey (faults are not shown).

sinistral and dextral movements, including the main Dardvey fault, have affected the Sangan prospect and have split the orebodies.

The Sangan prospect is dominated by the Cenozoic felsic subvolcanic intrusions and volcanic rocks, and of thick, weekly metamorphosed siliciclastic sedimentary rocks successions of Jurassic age, and Cretaceous carbonate rocks. Magmatism at the Sangan area commenced with the eruption of volcanic rocks, and was closely followed by the emplacement of granitoid porphyries consisting of granite, granodiorite, monzonite, diorite, and alkali feldspar granites (syenite, syenogranite, etc.) plutons, stocks, and dikes. Crosscutting relationships, and the absence or presence of skarn mineralization at the contact of the intrusions, suggest that the monzonite to quartz monzonites/syenites were emplaced before the mineralization took place. The quartz alkali syenite to quartz syenite, and the syenogranites exhibit iron skarn mineralization at their contact and are here assigned as the source intrusions. Volcanic rocks are largely exposed in the southern parts of the Sangan district and mainly consist of acid to intermediate and occasionally mafic rocks that are composed of rhyodacite, dacite, andesite–dacite, andesite, pyroxene andesite to basalt. Jurassic formations are the oldest geological units that cropout in the central mine areas where they strike E–W, and consist of shale and sandstone that are silicified at the contact with Cenozoic intrusions (Fig. 2).

## 4. Host and intrusive rocks

Host rocks at Sangan consist of recrystallized carbonate rocks of Cretaceous age that consist of limestone in the west, and dolomitic limestone in the east. A large syenite to syenogranite porphyry intrusion intrudes the Jurassic and the Cretaceous formations in the northern areas of the Sangan deposit (Fig. 2) giving rise to the formation of hornfels in the siliceous Jurassic rocks, and to skarn and magnetite ore at the contact with the host Cretaceous carbonate rocks. Field relationships, as well as lacking skarn and magnetite mineralization at the contact of the monzonitic intrusions with the carbonate rocks, indicate that the monzonites are older, and are unrelated to the skarn mineralization. They have solely led to the recrystallization of the carbonate rocks at their contact. This could also be confirmed by the radiometric age results obtained on zircon as discussed below.

## 5. The source intrusive rocks

Skarn mineralization occurs at the contact of the biotite hornblende quartz alkali syenite porphyries, and the hornblende biotite syenogranite porphyries as evidenced on the surface, as well as in the boreholes (Fig. 3A, B). The source intrusions are pinkish gray with a porphyritic to glomeroporphyritic texture and have equal amounts of phenocrysts and ground mass.

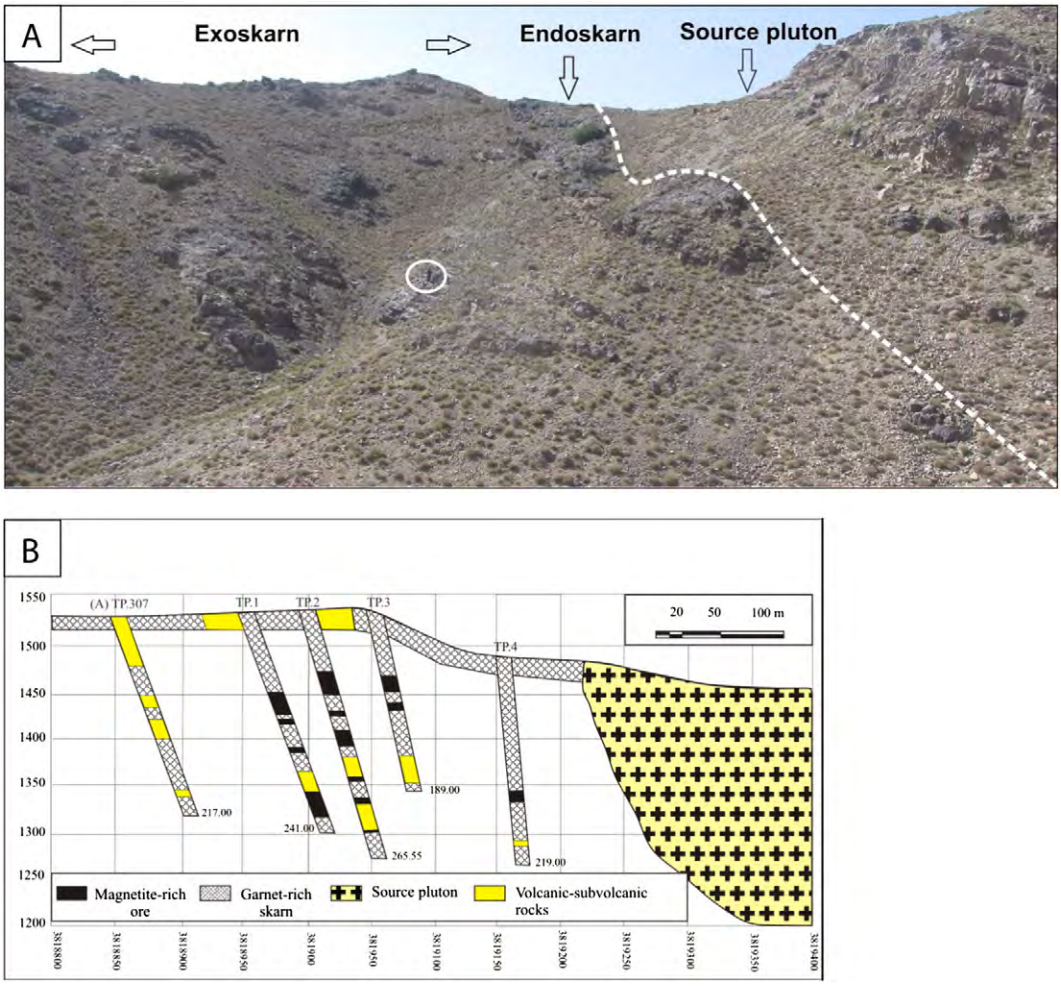


**Fig. 3.** A. Field photograph showing the spatial association of the source syenite-syenogranite porphyry pluton with skarn mineralization on the surface (for scale see person in circle), and (B) in the geological cross section at depth, both at Anomaly (Á).

(i) Biotite hornblende quartz alkali syenite porphyry
These rocks commonly occur as stocks and E–W trending small bodies in the area of the orebody (Á) and crosscut the older monzonite to quartz-monzonites. They are typified by a porphyritic texture and an abundance of euhedral to subhedral phenocrysts (>45%) consisting of 0.5–2.5 mm large plagioclase (~10%) and K-feldspar (~25%), hornblende (~7%), minor biotite (~1%) and quartz (~2%) in a medium grained matrix consisting of the same minerals. Accessory minerals are magnetite, zircon, and apatite. Locally, the hornblende and bitotite are replaced by chlorite, the feldspars are partially altered to sericite, and minor secondary quartz and calcite have been formed. The coarse grained varieties contain 20–25% plagioclase, 55–60% K-feldspar, 10–15% quartz, and 1–2% biotite and hornblende phenocrysts. Feldspar phenocrysts show weak sericitic alteration, although in places sericite becomes abundant.

(ii) Hornblende biotite syenogranite porphyry
The hornblende biotite syenogranite porphyries form the largest intrusions in the northeastern and eastern parts of the Sangan prospect. They exhibit a porphyric to granophyric texture, have a medium grained matrix, and contain more than 45%, 1–7 mm large phenocrysts that consist of plagioclase (~10%), K-feldspar (~25%), biotite (~5%), quartz (~5%), and minor hornblende (~1%). Accessory minerals are magnetite and zircon.

## 6. Geochemistry of the source intrusive rocks

### 6.1. Major elements

Major, trace and rare earth element data of the source intrusive rocks at Sangan prospect presented in Table 1 plot in the fields of quartz syenite and syenogranite of the Middlemost diagram (Fig. 4A). The $K_2O$ varies from 3.62 to 7.17 wt.%, and the $K_2O/Na_2O$ ratios between 0.90 and 2.47. The syenogranites represent high-K, subalkaline to shoshonite series, and the quartz alkali syenite to quartz syenite porphyries have shoshonitic affinity due to their high $K_2O$ (up to 6.5 wt.%). They are metaluminous to slightly peraluminous and their alumina saturation index-ASI (molar $Al_2O_3/(CaO + Na_2O + K_2O)$) remains below 1.1, which is the upper limit for the I-type granitoids (Chapell and White, 2001;

**Table 1**
Representative major and trace element data for the less altered source intrusive rock samples at Sagand. Major elements (analyzed by WD-XRD) are in wt.% and trace elements (analyzed by ICP-MS) in ppm.

| Sample location | 60°24′47″ 34°28′58″ | 60°25′00″ 34°30′10″ | 60°25′06″ 34°29′04″ | 60°25′05″ 34°29′08″ | 60°25′08″ 34°29′17″ | 60°24′52″ 34°29′25″ | 60°25′8″ 34°30′15″ | 60°25′04″ 34°29′45″ | 60°25′07″ 34°29′36″ | 60°25′05″ 34°29′35″ |
|---|---|---|---|---|---|---|---|---|---|---|
| Rock type | Biotite hornblende quartz alkali-syenite porphyry to hornblende quartz syenite porphyry | | | | Hornblende biotite syenogranite porphyry | | | | | |
| Sample no. | Stp-33 | Stp-34 | Stp-37 | Stp-75 DDH-TP13 | Stp-36 | Satp-119 DDH-71 | Saf-190 | Saf-192 | Saf-197 | Saf-198 |
| $SiO_2$ | 67.02 | 66.46 | 67.30 | 67.46 | 68.84 | 69.21 | 67.80 | 69.15 | 66.99 | 67.92 |
| $TiO_2$ | 0.43 | 0.44 | 0.33 | 0.34 | 0.43 | 0.32 | 0.34 | 0.32 | 0.46 | 0.46 |
| $Al_2O_3$ | 14.21 | 14.83 | 14.51 | 14.03 | 14.61 | 14.48 | 14.29 | 14.27 | 14.40 | 14.27 |
| FeOt | 2.39 | 2.56 | 2.18 | 2.52 | 2.29 | 2.57 | 3.03 | 2.97 | 3.99 | 2.94 |
| MnO | 0.06 | 0.05 | 0.03 | 0.06 | 0.03 | n.d | 0.04 | 0.02 | 0.02 | 0.02 |
| MgO | 1.42 | 0.43 | 1.08 | 1.47 | 0.52 | 0.34 | 1.52 | 1.32 | 1.84 | 1.63 |
| CaO | 2.61 | 3.73 | 2.53 | 2.33 | 2.67 | 2.21 | 2.43 | 1.49 | 2.28 | 3.79 |
| $Na_2O$ | 3.42 | 3.02 | 2.90 | 2.95 | 4.19 | 3.36 | 3.62 | 3.66 | 3.71 | 4.02 |
| $K_2O$ | 7.05 | 6.73 | 7.17 | 6.97 | 4.75 | 5.41 | 4.85 | 4.99 | 4.51 | 3.62 |
| $P_2O_5$ | 0.15 | 0.11 | 0.08 | 0.08 | 0.11 | 0.06 | 0.09 | 0.07 | 0.15 | 0.15 |
| $K_2O/Na_2O$ | 2.06 | 2.23 | 2.47 | 2.36 | 1.13 | 1.61 | 1.34 | 1.36 | 1.22 | 0.90 |
| Ba | 1097 | 1118 | 1400 | 1396 | 865 | 467 | 678 | 656 | 775 | 710 |
| Co | 1.5 | 1.2 | 0.7 | 0.5 | 1.4 | 0.3 | 2.4 | 2.4 | 3.8 | 1.4 |
| Cs | 0.8 | 0.7 | 0.9 | 0.9 | 0.7 | 1 | 0.8 | 0.9 | 1.2 | 0.6 |
| Ga | 20 | 19 | 18 | 17 | 19 | 18 | 19 | 20 | 20 | 19 |
| Hf | 7 | 9 | 6 | 6 | 8 | 8 | 10 | 10 | 7 | 9 |
| Nb | 24 | 26 | 19 | 20 | 26 | 30 | 31 | 33 | 24 | 26 |
| Rb | 192 | 186 | 189 | 195 | 134 | 155 | 169 | 163 | 157 | 101 |
| Sr | 173 | 212 | 127 | 96 | 212 | 115 | 139 | 148 | 277 | 362 |
| Ta | 1.7 | 1.8 | 1.6 | 1.4 | 1.7 | 2.3 | 2.3 | 2.6 | 1.6 | 2 |
| Th | 25 | 28 | 26 | 26 | 27 | 33 | 35 | 38 | 26 | 25 |
| V | 53 | 32 | 20 | 22 | 34 | 10 | 16 | 16 | 40 | 40 |
| Zr | 311 | 335 | 277 | 259 | 335 | 255 | 394 | 342 | 296 | 381 |
| Y | 26 | 30 | 23 | 23 | 30 | 27 | 39 | 39 | 30 | 31 |
| La | 43.4 | 47.2 | 50.4 | 93.3 | 79.7 | 41.8 | 107.1 | 89.2 | 59.5 | 55.4 |
| Ce | 102.2 | 117.2 | 94.5 | 162.7 | 148.1 | 88.8 | 187.4 | 170.5 | 122.4 | 122 |
| Pr | 11.5 | 13.2 | 10.5 | 16.0 | 14.8 | 9.9 | 18.1 | 17.2 | 12.7 | 13.2 |
| Nd | 41.9 | 48.3 | 35.6 | 51.1 | 48.7 | 34.1 | 56.3 | 58.9 | 45.9 | 49.3 |
| Sm | 6.9 | 7.6 | 6.0 | 7.5 | 7.8 | 6.0 | 9.0 | 9.7 | 7.5 | 8.5 |
| Eu | 0.9 | 1.4 | 1.1 | 1.4 | 1.5 | 0.9 | 1.3 | 1.3 | 1.4 | 1.62 |
| Gd | 5.4 | 6.7 | 4.8 | 5.4 | 6.0 | 5.0 | 7.3 | 7.6 | 6.1 | 6.6 |
| Tb | 0.9 | 1.0 | 0.7 | 0.7 | 0.9 | 0.8 | 1.1 | 1.1 | 0.9 | 0.9 |
| Dy | 4.9 | 5.40 | 3.61 | 4.48 | 5.28 | 4.54 | 6.43 | 7.02 | 5.36 | 5.80 |
| Ho | 1.02 | 1.0 | 0.8 | 0.8 | 1.1 | 1.0 | 1.4 | 1.3 | 1.0 | 1.0 |
| Er | 2.9 | 3.0 | 2.2 | 2.2 | 3.0 | 2.9 | 3.5 | 4.0 | 2.9 | 2.9 |
| Tm | 0.4 | 0.5 | 0.3 | 0.4 | 0.5 | 0.44 | 0.53 | 0.65 | 0.41 | 0.41 |
| Yb | 3.2 | 3.4 | 2.0 | 1.9 | 2.8 | 3.2 | 4.0 | 4.3 | 3.2 | 3.3 |
| Lu | 0.4 | 0.5 | 0.4 | 0.4 | 0.4 | 0.4 | 0.5 | 0.6 | 0.4 | 0.5 |
| $(La/Yb)_N$ | 9.26 | 9.39 | 16.82 | 32.42 | 19.26 | 8.78 | 17.83 | 13.99 | 12.50 | 11.22 |
| Eu/Eu | 0.44 | 0.61 | 0.65 | 0.69 | 0.70 | 0.50 | 0.48 | 0.48 | 0.65 | 0.66 |

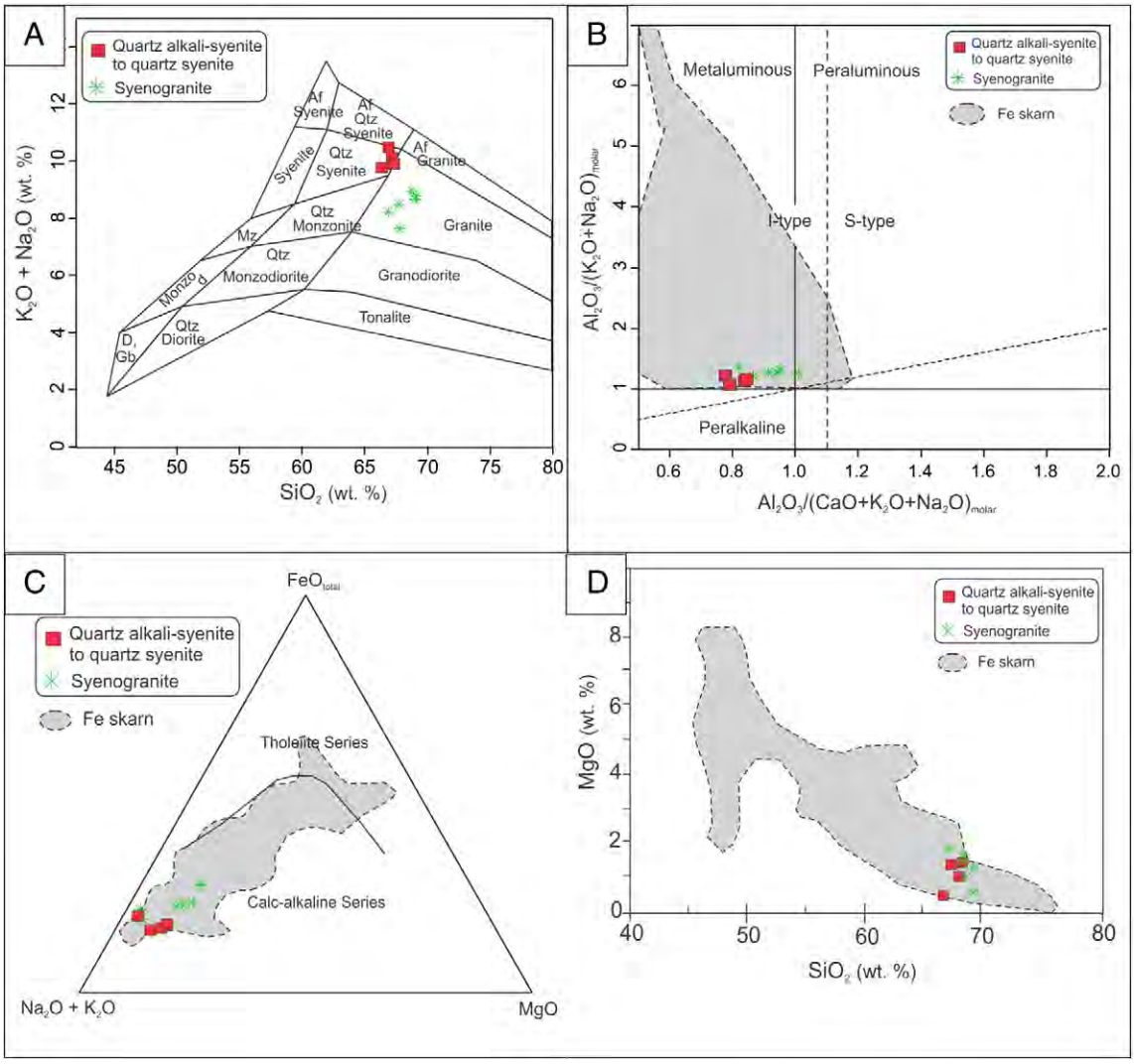


**Fig. 4.** A. Geochemical classification of the source intrusive rocks from Sangan deposit in a) $Na_2O + K_2O$ vs. $SiO_2$ diagram of Middlemost (1994), b) in $Al_2O_3/Na_2O + K_2O$ vs. $Al_2O_3/CaO + K_2O + Na_2O$ diagram of Maniar and Piccoli (1989). Dash line (A/CNK = 1.1) separates the I-type (A/CNK < 1.1) and S-type (A/CNK > 1.1) fields (from Chapell and White, 2001); C) in AFM diagram showing the source intrusive rocks for Sangan deposits (calcalkaline-tholeiitic boundary line is from Irvine and Baragar, 1971), and D) MgO vs. $SiO_2$ diagram for the same rocks. Composition of the global igneous rocks associated with the iron skarn deposits (from Meinert, 1995) are shown for comparison.

Fig. 4B). These intrusions also show calcalkaline affinity (Fig. 4C) with chemical characteristics similar to the intrusive rocks associated with global iron skarns. In $SiO_2$ versus MgO diagram (Fig. 4D), the syenite and syenogranite samples plot in the more differentiated field with high $SiO_2$ and low MgO, likewise similar to the igneous rocks associated with the iron skarns (Meinert, 1995).

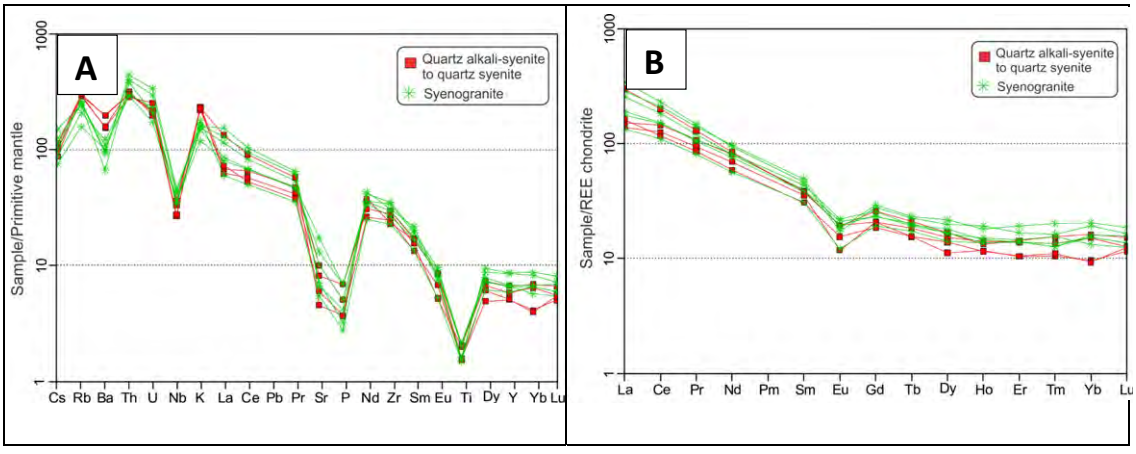


**Fig. 5.** A. Primitive mantle normalized trace element pattern for Sangan source intrusive rocks (values from Sun and McDonough, 1989), and B) chondrite normalized REE patterns (values from Boynton, 1984) for the same rocks.

### 6.2. Trace and rare earth elements

The source syenitic and granosyenitic intrusions have similar primitive mantle normalized trace element pattern, are enriched in large ion lithophile (LILE, Cs, Rb, Ba, K), in incompatible elements that behave similar to LILE (Th, U), in LREE (La, Ce), and are strongly depleted in high field strength elements (HFSE, Nb, Y, Ti) and HREE (Yb, Lu) compared to the primitive mantle (Fig. 5A, B). These features are typical of the subduction related magmas in the calcalkaline volcanic arcs of continental active margins (Gill, 1981; Pearce, 1983; Walker et al., 2001; Wilson, 1989). Their low Sr, Nb, Ta, and Ti contents are thought to be due to the presence of plagioclase and Fe–Ti oxides, or Ti (Nb) minerals (rutile and ilmenite) in the residue left in the source area of the parental magmas (Martin, 1999; Pearce and Parkinson, 1993; Reagan and Gill, 1989). Nb and Ta contents may also be viewed as resulting from a previous depletion in the mantle source rocks (Gust et al., 1997; Woodhead et al., 1993). The source intrusive rocks show similar chondrite normalized REE patterns with highly fractionated REE and moderate LREE enrichment ($32.42 \geq La_N/Yb_N \geq 8.78$), and Eu/Eu* [$Eu_{cn}/(Sm_{cn} \times Gd_{cn})^{0.5}$] ratios varying from 0.44 to 0.70 that accounts for negative Eu anomaly.

## 7. U–Pb zircon ages

U–Pb ages were determined on zircon separates from two representative source rock samples (i) biotite hornblende quartz alkali syenite porphyry (sample Stp-34), and (ii) hornblende biotite syenogranite porphyry (sample Saf-197) from the area of Anomaly (Á). Dated zircon grains were colorless and/or pale yellow, transparent and commonly euhedral, mostly with oscillatory zoning. The grain sizes ranged from 50–300 μm with a length to width ratio of 1:1 to 5:1.

The result of the calculated isotopic zircon ages (Tables 2 and 3) is presented as Concordia and average age graphics in Fig. 6A, B, C, D. The mean ages (weighted mean) are 39.1 ± 0.6 Ma for sample Stp-34 on the basis of 21 analyzed points, and 38.3 ± 0.5 Ma for sample Saf-197 on the basis of 23 analyzed points (errors shown are 2$\sigma$). The relatively constant U/Th ratios and their respective U–Pb ages are consistent with magmatic zircons, and no inherited components were detected. These characteristics together with the high closure temperatures of zircon (Cherniak and Watson, 2000) allow us to interpret the U–Pb data as representative of the crystallization ages of the respective igneous rocks indicating that the intrusion occurred in the Middle Eocene (Bartonian). These ages are in agreement with the radiometric U–Pb zircon ages obtained by Malekzadeh Shafaroudi et al. (2013) for three intrusive rocks from Baghak and (Cn). The obtained ages also resulted in distinction of three intrusion pulses consisting of (i) a 42.3 Ma biotite hornblende quartz monzonite porphyry to biotite syenogranite porphyry, (ii) a 40 Ma biotite quartz monzonite porphyry to biotite syenogranite porphyry, and (iii) a 39.2 Ma hornblende biotite syenogranite porphyry. The (i) and (ii) intrusions are pre-mineralization, whereas the group (iii) intrusions represent the source rocks.

## 8. Skarn-iron orebodies

The Sangan deposit consists of seven iron oxide orebodies, or anomalies named at the mine as (Á), (A), (B), and C-South (Cs) in the western sector, and C-North (Cn), Baghak and Dardvey in the eastern sector that occur along a 8 km E–W striking zone in the Cretaceous carbonate rocks (Figs. 2 and 7A). The original E–W strike of the orebodies has been tectonically modified along the NNW to NW fault system; the (Á) is displaced to the north relative to (A), the (Cs) has been split from the (Cn), and the Baghak and Dardvey orebodies have been displaced over a distance of around 1 km (Fig. 7B). The thickness of the orebodies varies between 10 cm to 200 m, and they occur at depths down to 600 m below the surface. The largest iron ore tonnages at Sangan occur at orebodies (B; 235 Mt), and at Baghak (185 Mt), which is a massive magnetite of around 400 m length and 250 m width (for ore reserves see Table 11).

The iron-skarn mineralization consists of stratiform, tabular layers to massive bodies, lenses, and laminas of magnetite with minor amounts of sulfides that alternate, or is intergrown with calcsilicate skarn minerals. The primary texture of the host rocks is locally preserved, and is clearly visible as interlayering of the magnetite ore with dolostone in the outcrops east of Dardvey Anomaly. The field exposures, as well as the data from the study of the bore holes show recrystallization and skarnization only at the contact of the source quartz alkali syenite to syenogranite porphyries with the Cretaceous carbonate rocks, and the formation of hornfels at the contact with Jurassic siliciclastic rocks. The intrusive rocks occur in limited surface outcrops at Anomaly (Á), where abundant garnet skarn and iron ore has been formed at their contact, but are extensively found in the drill cores at the orebodies (Á) and Dardvey. The eastern anomalies (Cn), Baghak, and Dardvey are therefore regarded as distal skarns. The skarns at Sangan consist of endoskarns, and exoskarns, whereas the magnetite is associated with the exoskarns.

**Table 2**
Results of U–Pb–Th laser-ablation multicollector ICP mass spectrometry analysis of zircon from the biotite hornblende quartz alkali-syenite porphyry (sample Stp-34).

| Analysis | U (ppm) | $^{206}Pb/^{204}Pb$ | U/Th | $^{206}Pb/^{207}Pb$ | ± (%) | $^{207}Pb/^{235}U$ | ±(%) | $^{206}Pb/^{238}U$ | ±(%) | Age (Ma) | ±(Ma) |
|---|---|---|---|---|---|---|---|---|---|---|---|
| 1 | 99 | 1444 | 0.6 | 22.3896 | 4.3 | 0.0363 | 4.5 | 0.0059 | 1.5 | 37.9 | 0.6 |
| 2 | 191 | 4655 | 0.9 | 21.1741 | 1.6 | 0.0385 | 2.2 | 0.0059 | 1.6 | 38.0 | 0.6 |
| 3 | 154 | 2919 | 0.6 | 22.2146 | 2.1 | 0.0368 | 3.9 | 0.0059 | 3.4 | 38.1 | 1.3 |
| 4 | 111 | 2477 | 1.0 | 21.1590 | 3.0 | 0.0387 | 3.3 | 0.0059 | 1.4 | 38.2 | 0.5 |
| 5 | 120 | 2610 | 0.7 | 21.7116 | 2.9 | 0.0380 | 3.4 | 0.0060 | 1.7 | 38.5 | 0.7 |
| 6 | 83 | 2091 | 0.8 | 22.0202 | 1.8 | 0.0375 | 2.5 | 0.0060 | 1.7 | 38.5 | 0.7 |
| 7 | 125 | 10276 | 0.6 | 20.4590 | 2.8 | 0.0404 | 3.1 | 0.0060 | 1.3 | 38.6 | 0.5 |
| 8 | 108 | 15007 | 0.9 | 20.8843 | 2.9 | 0.0398 | 3.6 | 0.0060 | 2.1 | 38.7 | 0.8 |
| 9 | 82 | 1586 | 0.6 | 21.6484 | 7.3 | 0.0385 | 7.4 | 0.0061 | 1.0 | 38.9 | 0.4 |
| 10 | 133 | 4023 | 0.8 | 21.2126 | 1.9 | 0.0394 | 2.4 | 0.0061 | 1.4 | 38.9 | 0.6 |
| 11 | 135 | 3995 | 1.0 | 21.3054 | 2.2 | 0.0396 | 2.8 | 0.0061 | 1.7 | 39.3 | 0.7 |
| 12 | 61 | 1873 | 0.7 | 21.0665 | 4.0 | 0.0401 | 5.6 | 0.0061 | 3.9 | 39.4 | 1.5 |
| 13 | 97 | 7842 | 0.8 | 19.7911 | 3.7 | 0.0430 | 4.1 | 0.0062 | 1.8 | 39.7 | 0.7 |
| 14 | 27 | 882 | 0.8 | 20.8992 | 7.9 | 0.0408 | 8.6 | 0.0062 | 3.3 | 39.7 | 1.3 |
| 15 | 133 | 3998 | 0.8 | 21.5207 | 3.4 | 0.0397 | 3.6 | 0.0062 | 1.1 | 39.8 | 0.4 |
| 16 | 67 | 1979 | 0.9 | 20.8114 | 3.5 | 0.0411 | 3.5 | 0.0062 | 0.7 | 39.8 | 0.3 |
| 17 | 142 | 3241 | 0.9 | 21.7077 | 3.6 | 0.0396 | 3.9 | 0.0062 | 1.6 | 40.1 | 0.6 |
| 18 | 196 | 7177 | 0.6 | 20.8294 | 2.1 | 0.0414 | 2.6 | 0.0062 | 1.4 | 40.1 | 0.6 |
| 19 | 111 | 3883 | 0.7 | 20.8599 | 3.1 | 0.0419 | 4.3 | 0.0063 | 3.0 | 40.7 | 1.2 |
| 20 | 854 | 17059 | 1.9 | 21.3466 | 1.3 | 0.0413 | 1.9 | 0.0064 | 1.3 | 41.1 | 0.5 |
| 21 | 73 | 1496 | 0.9 | 22.3245 | 4.4 | 0.0397 | 4.6 | 0.0064 | 1.3 | 41.3 | 0.5 |

**Table 3**
Results of U–Pb–Th laser-ablation multicollector ICP mass spectrometry analysis of zircon from the hornblende biotite syenogranite porphyry (sample Saf-197).

| Analysis | U (ppm) | $^{206}Pb/^{204}Pb$ | U/Th | $^{206}Pb/^{207}Pb$ | ±(%) | $^{207}Pb/^{235}U$ | ±(%) | $^{206}Pb/^{238}U$ | ±(%) | Age (Ma) | ±(Ma) |
|---|---|---|---|---|---|---|---|---|---|---|---|
| 1 | 55 | 1083 | 0.9 | 21.6114 | 5.4 | 0.0366 | 5.6 | 0.0057 | 1.7 | 36.9 | 0.6 |
| 2 | 39 | 1738 | 0.5 | 18.6564 | 3.3 | 0.0427 | 5.8 | 0.0058 | 4.8 | 37.1 | 1.8 |
| 3 | 37 | 969 | 0.6 | 20.9576 | 10.5 | 0.0380 | 11.0 | 0.0058 | 3.2 | 37.1 | 1.2 |
| 4 | 123 | 1571 | 0.7 | 22.8777 | 3.8 | 0.0350 | 4.4 | 0.0058 | 2.2 | 37.3 | 0.8 |
| 5 | 153 | 2615 | 0.9 | 14.0124 | 42.5 | 0.0573 | 42.8 | 0.0058 | 4.9 | 37.4 | 1.8 |
| 6 | 180 | 5296 | 0.7 | 21.4277 | 1.8 | 0.0375 | 3.8 | 0.0058 | 3.3 | 37.5 | 1.2 |
| 7 | 119 | 1806 | 0.8 | 21.2218 | 3.4 | 0.0380 | 5.1 | 0.0058 | 3.9 | 37.6 | 1.4 |
| 8 | 140 | 3787 | 0.7 | 20.9231 | 3.2 | 0.0387 | 4.0 | 0.0059 | 2.4 | 37.7 | 0.9 |
| 9 | 135 | 3075 | 0.7 | 20.8464 | 2.7 | 0.0389 | 3.8 | 0.0059 | 2.6 | 37.8 | 1.0 |
| 10 | 127 | 1834 | 0.7 | 22.7112 | 2.1 | 0.0360 | 2.4 | 0.0059 | 1.1 | 38.1 | 0.4 |
| 11 | 231 | 3376 | 0.4 | 21.7083 | 2.2 | 0.0377 | 2.9 | 0.0059 | 1.9 | 38.1 | 0.7 |
| 12 | 57 | 1562 | 0.8 | 20.8837 | 6.8 | 0.0393 | 7.3 | 0.0060 | 2.5 | 38.3 | 0.9 |
| 13 | 515 | 26406 | 0.7 | 20.8254 | 2.0 | 0.0395 | 4.0 | 0.0060 | 3.5 | 38.4 | 1.3 |
| 14 | 143 | 1492 | 0.9 | 22.6022 | 2.7 | 0.0365 | 4.4 | 0.0060 | 3.6 | 38.4 | 1.4 |
| 15 | 67 | 1238 | 0.9 | 23.1732 | 5.9 | 0.0356 | 6.0 | 0.0060 | 1.1 | 38.5 | 0.4 |
| 16 | 238 | 3762 | 0.7 | 21.1526 | 2.1 | 0.0391 | 3.0 | 0.0060 | 2.1 | 38.6 | 0.8 |
| 17 | 165 | 4978 | 0.7 | 21.1577 | 2.6 | 0.0392 | 3.2 | 0.0060 | 1.9 | 38.6 | 0.7 |
| 18 | 126 | 2511 | 0.7 | 21.3246 | 3.5 | 0.0389 | 4.0 | 0.0060 | 2.0 | 38.7 | 0.8 |
| 19 | 149 | 1997 | 0.7 | 21.5280 | 2.4 | 0.0392 | 3.0 | 0.0061 | 1.8 | 39.3 | 0.7 |
| 20 | 165 | 4635 | 0.7 | 20.3954 | 2.0 | 0.0414 | 2.4 | 0.0061 | 1.3 | 39.3 | 0.5 |
| 21 | 251 | 4794 | 0.8 | 20.7466 | 3.0 | 0.0409 | 4.1 | 0.0062 | 2.8 | 39.6 | 1.1 |
| 22 | 150 | 2635 | 0.8 | 20.8935 | 3.8 | 0.0409 | 4.2 | 0.0062 | 1.8 | 39.9 | 0.7 |
| 23 | 137 | 3370 | 0.7 | 19.9160 | 6.6 | 0.0453 | 7.1 | 0.0065 | 2.6 | 42.0 | 1.1 |

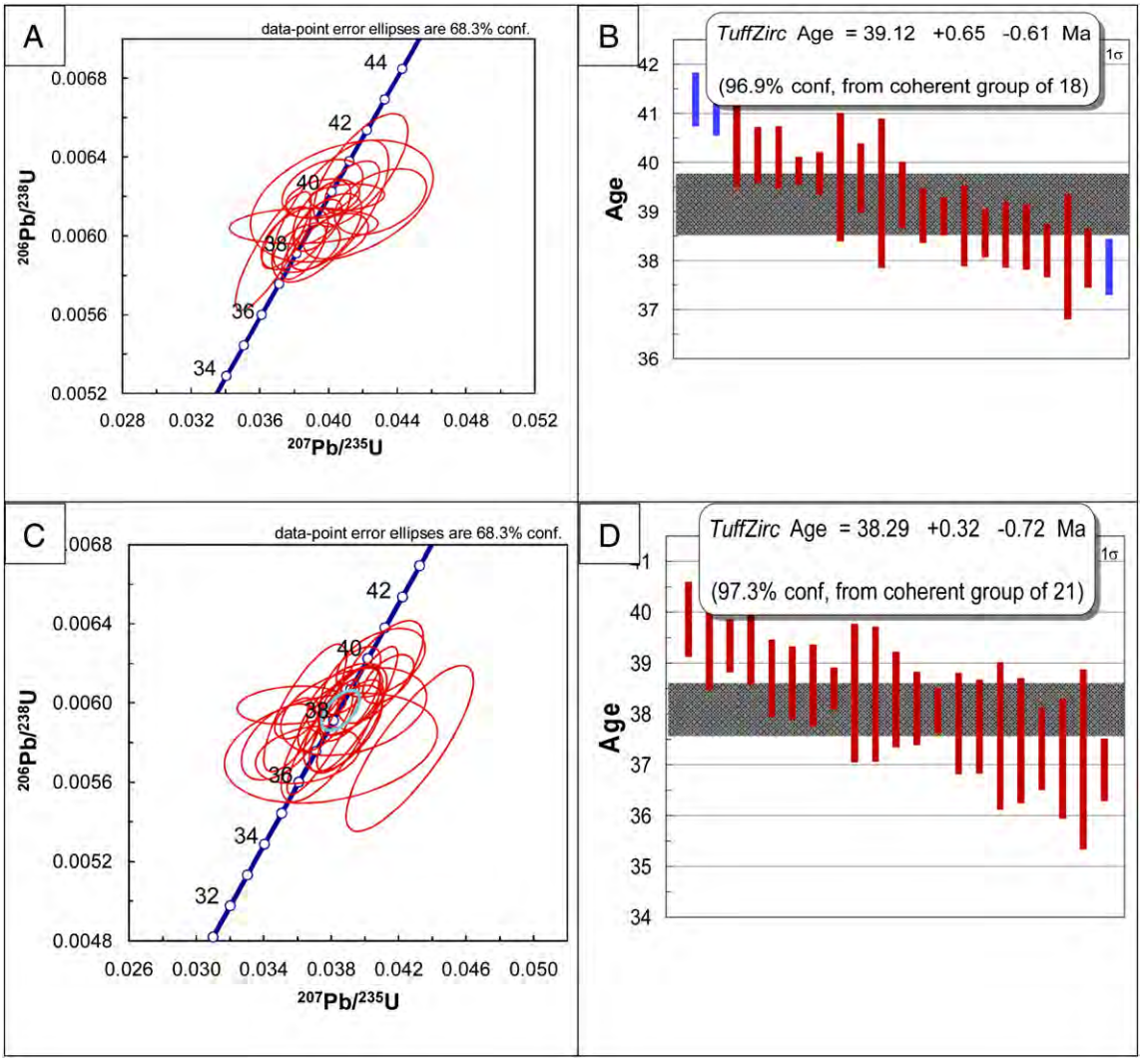


**Fig. 6.** A. The average age plot, and B) the Concordia diagram for biotite-hornblende-quartz-alkali syenite; C) the average age plot, and D) the Concordia diagram for the hornblende-biotite syenogranite of the Sangan deposit.

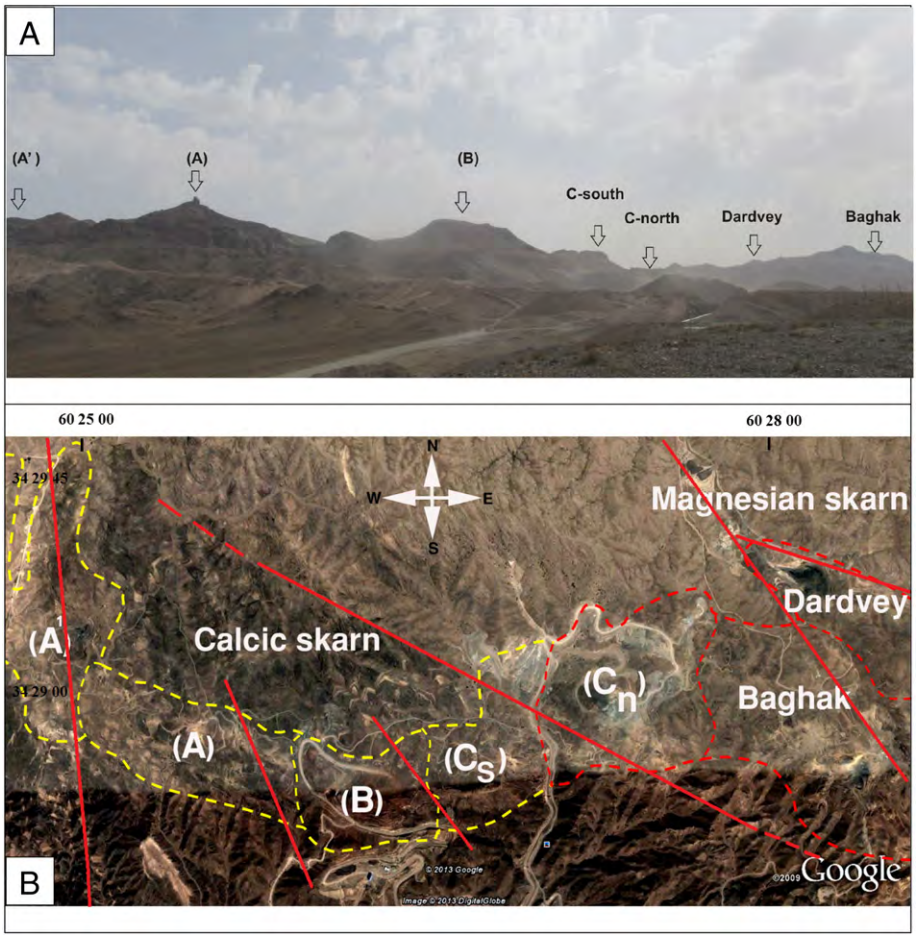


**Fig. 7.** A. View looking north of the Sangan deposit showing the iron skarn Anomalies (Á), (A), (B), C-north, C-south, Baghak, and Dardvey along an 8 km E-W striking zone, and B) the surface exposure of the eastern calcic and the western magnesian skarns with displacement of the orebodies (Á) relative to (A), (Cs) relative to (Cn), and Dardvey relative to Baghak, along the NNW to NW fault system.

The skarn mineralogy directly follows the composition of the host carbonate rocks: the limestone-hosted, western skarns are typically calcic, whereas the skarns in the eastern dolostones are typically magnesian. The gradational change from the calcic to the magnesian skarns can be followed from the west to the east by the presence of large amounts of phlogopite, serpentine, and talk in transitional zone at (Cs), particularly at depth.

### 8.1. Skarn mineralogy and mineral chemistry

#### 8.1.1. Western calcic skarns

The western calcic iron skarns (Á), (A), (B), and part of the (Cs) consist of abundant garnet with amphibole, chlorite, and lesser amounts of pyroxene and the magnetite ore. Garnet is the main skarn mineral after the magnetite and can be found in the immediate vicinity of the syenitic intrusions with the Cretaceous limestone. Garnet commonly forms large, brown-reddish pentagon dodecahedrons of over 1 cm (Fig. 8A, B) and is commonly associated with calcite in intragranular fillings between garnet crystals, or as late veinlets (Fig. 8A, C, E, F, G, H). Garnet grains show anomalous anisotropy under the microscope (Fig. 8C). Composition of the most garnet grains determined by the electron microprobe is andradite to grossular (Table 4; Fig. 9) with trace amounts of Mn and Mg ($Adr_{50-97}Grs_{0-45}Sps\text{-}Alm_{2-7}$). Compositional changes from 58–60% andradite in the core part to more than 97% andradite in the periphery of the garnet grain, is reflected in the common optical zoning. Calcite and quartz are late (Fig. 8C) and generally occur as crosscutting veinlets, and late calcite fillings.

Clinopyroxene, a common skarn mineral in almost all Sangan orebodies, is less abundant than garnet, and is largely converted to amphibole during the retrograde alteration, in particular at western anomalies (Fig. 8D). The average composition of the pyroxene determined by electron microprobe is $Hd_{75.6}Di_{20}Jo_{4.5}$ (Table 5 and Fig. 10). Amphibole is common at Sangan, and is in particular abundant in the western anomalies. It commonly occurs as, 1–10 cm long, greenish to black, elongated crystal aggregates of actinolite that have been formed due to the retrograde metasomatism of the pyroxene (Fig. 8E, F and G). Electron microprobe analyses indicate the high Ca and Fe contents of the amphiboles (Table 6). Prograde amphibole from the endoskarn (Anomaly Á) plot in the field of F–Cl-bearing ferroactinolite, and the amphiboles from the exoskarns plot in the field of ferrohastingsite (Fig. 11). The endoskarn at (Á) is additionally associated with high temperature minerals wollastonite, plagioclase, and K-feldspar. Chlorite, also a common mineral at Sangan, is a retrograde metasomatic mineral with an Fe-rich chlorite composition (ripidolite), and is more abundant in the western anomalies (Table 7; Figs. 8G, H and 12).

#### 8.1.2. Eastern magnesian skarns

The magnesian skarn on the surface outcrops of the eastern sector consists of exoskarns with prograde forsterite ($Fo_{97.0}Fa_{2.7}$; Table 8), diopsidic pyroxene ($Hd_{0.2}Di_{0.88}$; see Table 5 and Fig. 10), and some escapolite that are associated with abundant phlogopite, in particular at Baghak and Dardvey, and retrograde Mg-rich actinolite (see Table 6, and Fig. 10), chlorite (see Table 7, and Fig. 12), serpentine, and talc (Fig. 13A, B, C, D, E, F). Phlogopite forms dark green, large sheets of up

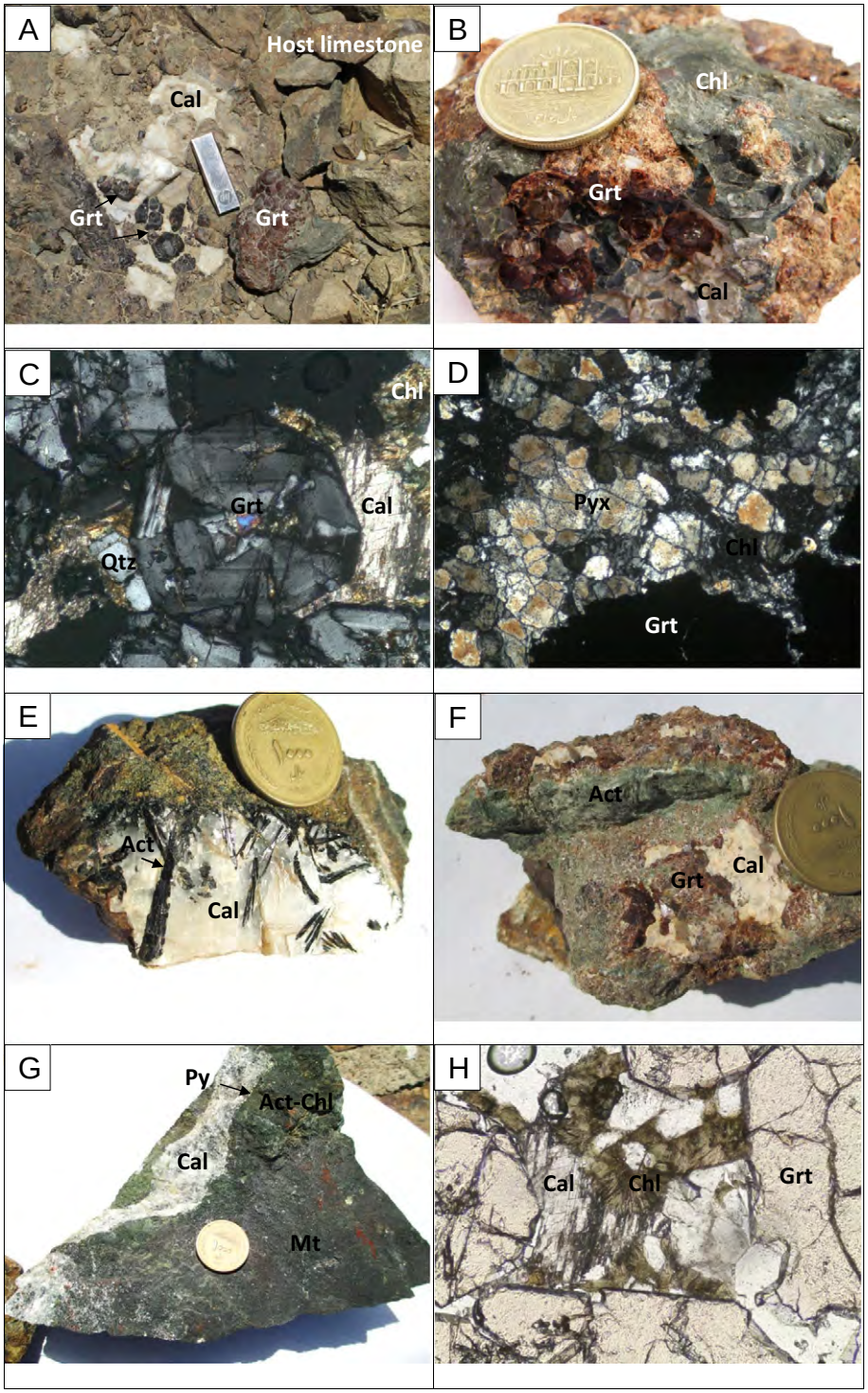


**Fig. 8.** Field, handspecimen, and microphotographs from the western calcic skarn Tappeh Ghermez, Anomlay (Á) showing, A) and B) dark red-brown pentagon dodecahedron crystals of garnet in white calcite; C) zoned andradite-grossular garnet with anomalous anisotropy in a matrix of calcite (rhombic cleavage), late quartz, and chlorite (width of the photograph is 1.2 mm); D) fine grained aggregates of pyroxene altered to chlorite and associated with garnet (width of the photograph 1.2 mm); E) dark green, elongated crystal aggregates of actinolite protruding into late white calcite with rhombic cleavage; F) light green, retrograde actinolite-chlorite formed from pyroxene in a garnet skarn; G) retrograde chlorite with massive magnetite ore. A thin film of pyrite occurs on the wall of the late veinlet calcite; h) retrograde chlorite with green-brown pleochroism in intragranular spaces of garnet together with calcite (rhombic cleavages) (width of the microphotograph is 1.2 mm). Act: actinolite; Cal: calcite; Chl: chlorite; Grt: garnet;Py: pyrite; Pyx: pyroxene; Qtz: quartz.

to 20 cm and larger (Fig. 13C, D, E), and is commonly closely associated with the magnetite ore (Fig. 13C, D). Electron microprobe analyses show low Fe- and F- contents of the phlogopite (Table 9). In contrast to Fe-rich chlorites of the western skarns, the chlorites from the eastern skarns consist of Mg-rich clinochlore (see Table 7, and Fig. 12). Minor late quartz occurs as veinlets crosscutting other skarn minerals, and calcite is uncommon. No endoskarns were observed on the surface at the eastern sector.

*8.1.3. Ore mineralogy and mineral chemistry*

The economic ore mineral at Sangan is magnetite that makes up to >95% of the total ore minerals that are associated with minor amounts

**Table 4**
Representative microprobe analyses of garnet from the western calcic skarn (Á).

| wt.% | SK-4 | SK-4 | SK-7 | SK-7 | SK-7 | KÁ-3 © | KÁ-3 ® | KÁ-4 © | KÁ-4 ® | KÁ-7 | KÁ-7 |
|---|---|---|---|---|---|---|---|---|---|---|---|
| $SiO_2$ | 36.51 | 37.21 | 36.81 | 36.70 | 37.48 | 36.75 | 35.44 | 36.50 | 34.99 | 36.55 | 36.81 |
| $TiO_2$ | 0.03 | 0.10 | 0.05 | – | 0.36 | 0.12 | 0.09 | 0.08 | – | 0.17 | 0.23 |
| $Al_2O_3$ | 6.43 | 10.57 | 10.6 | 10.48 | 10.48 | 8.65 | 3.48 | 8.10 | 0.34 | 8.42 | 8.76 |
| $Fe_2O_3$ | 22.66 | 16.75 | 16.88 | 16.87 | 16.95 | 19.27 | 26.39 | 20.19 | 31.11 | 19.34 | 19.03 |
| FeO | 1.12 | 1.76 | 1.54 | 1.60 | 1.04 | 2.00 | 0.92 | 1.47 | 0.59 | 1.65 | 1.56 |
| MnO | 0.60 | 0.88 | 0.95 | 1.09 | 1.08 | 1.23 | 0.59 | 0.95 | 0.44 | 0.89 | 1.07 |
| MgO | – | – | – | 0.01 | – | 0.03 | – | 0.05 | 0.04 | 0.06 | 0.07 |
| CaO | 33.54 | 33.24 | 33.80 | 33.79 | 33.90 | 32.49 | 36.30 | 33.41 | 32.75 | 32.73 | 32.82 |
| $Na_2O$ | – | – | 0.01 | – | – | – | 0.02 | – | – | – | – |
| $K_2O$ | – | – | – | – | – | – | – | – | 0.013 | – | – |
| F | 0.02 | 0.12 | 0.18 | – | 0.16 | – | 0.22 | – | 0.14 | – | 0.05 |
| Total | 100.92 | 100.64 | 100.82 | 100.57 | 101.46 | 100.57 | 99.39 | 100.75 | 100.42 | 99.82 | 100.41 |
| * | 1 | 1 | 1 | 1 | 1 | 1 | 1 | 0.97 | 1 | 0.97 | 0.94 |
| *Numbers of cations on the basis of 24 O* | | | | | | | | | | | |
| Si | 5.94 | 5.95 | 5.88 | 5.89 | 5.93 | 5.95 | 5.94 | 5.91 | 5.91 | 5.95 | 5.94 |
| Ti | – | 0.01 | – | – | 0.04 | 0.014 | 0.01 | – | – | 0.02 | 0.3 |
| Al | 1.23 | 1.99 | 1.98 | 1.98 | 1.95 | 1.65 | 0.69 | 1.55 | 0.07 | 1.61 | 1.67 |
| $Fe^{3+}$ | 2.78 | 2.01 | 2.03 | 2.04 | 2.02 | 2.35 | 3.33 | 2.46 | 3.96 | 2.37 | 2.31 |
| $Fe^{2+}$ | 0.15 | 0.23 | 0.21 | 0.21 | 0.14 | 0.27 | 0.13 | 0.20 | 0.08 | 0.23 | 0.21 |
| Mn | 0.08 | 0.12 | 0.13 | 0.15 | 0.15 | 0.17 | 0.08 | 0.13 | 0.06 | 0.12 | 0.15 |
| Mg | – | – | – | – | – | – | – | 0.01 | – | 0.01 | 0.02 |
| Ca | 5.85 | 5.69 | 5.79 | 5.81 | 5.75 | 5.63 | 5.8 | 5.80 | 5.93 | 5.71 | 5.68 |
| Na | – | – | – | – | – | – | – | – | – | – | – |
| K | – | – | – | – | – | – | – | – | – | – | – |
| *Endmember* | | | | | | | | | | | |
| Adr | 68.52 | 50.21 | 49.85 | 49.53 | 51.04 | 58.18 | 83.26 | 60.33 | 97.45 | 58.98 | 57.90 |
| Grs | 27.62 | 43.91 | 44.68 | 44.56 | 44.24 | 34.44 | 13.16 | 34.10 | – | 35.04 | 35.91 |
| Prp | – | – | – | 0.05 | – | 0.14 | 0.04 | 0.20 | 0.15 | 0.23 | 0.28 |
| Sps | 1.35 | 1.98 | 2.11 | 2.39 | 2.42 | 2.77 | 1.40 | 2.13 | 1.03 | 2.03 | 2.43 |
| Alm | 2.51 | 3.89 | 3.36 | 3.47 | 2.29 | 4.47 | 2.15 | 3.24 | 1.36 | 3.72 | 3.48 |

*$(Fe^{2+}+Mn)$ / $(Fe^{2+}+Mn+Mg)$; © = core; ® = rim; (−) = below detection limit.

of sulfides (Fig. 14A, B). Magnetite occurs as massive compact ore, and as disseminations in the low grade calcsilicate skarns in the calcic, as well as in the magnesian skarns. The magnetite ore consists of medium grained, euhedral to unhedral, commonly 1 mm large grains (Fig. 14C, D, E) that show a light beige color under reflected light microscope, apparently due to the presence of Ti. Electron microprobe analysis of the magnetite grains shows the presence of minor to trace amounts of $TiO_2$, MgO, CaO, MnO, NiO, and $Cr_2O_3$ in the magnetite (Table 10). Concentrations of MgO in the magnetite from the eastern orebodies that formed at the contact with dolostones are higher than in the western magnetites and reach values of up to 3.65%. Magnetite is oxidized to martite (<5%), and to goethite-limonite on the surface.

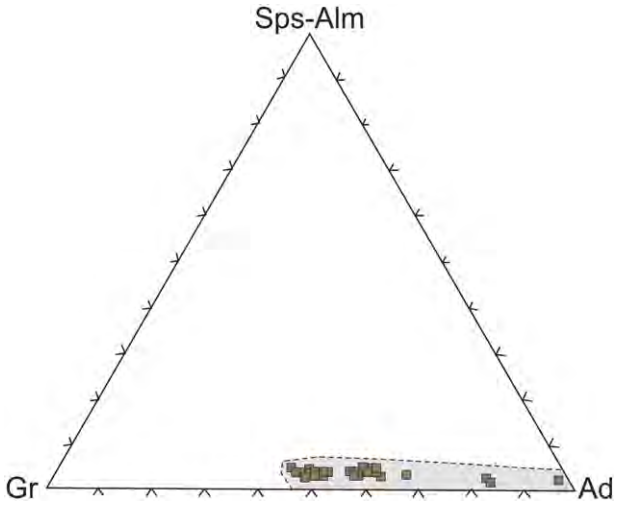


**Fig. 9.** Plot of microprobe analyses showing the compositional range of garnets from the western calcic skarn (Á) in andradite (Ad)-grossular (Gr)-spessartine-almandine (Sps-Alm) triangle.

The content of the sulfide minerals at Sangan is low and commonly increases from the western orebodies (S ≤ 2%) to the eastern orebodies (S ≥ 5%) and through depth. Sulfides are later and occur as crosscutting veins and veinlets of up to 2 m thick at depth in the magnetite ore. They consist of subordinate amounts of pyrite, chalcopyrite, and pyrrhotite. Early sulfides, commonly pyrite and chalcopyrite with occasional pyrrhotite, occur as disseminated grains with the magnetite (Fig. 14C, D, E, F). Pyrrhotite is in some cases replaced by pyrite (Fig. 14C, F). Chalcopyrite is closely associated with pyrite, and in some places with pyrrhotite, such as at Baghak. Occasionally (e.g., Anomaly-A), minor amounts of arsenopyrite occur, too, but Pb–Zn sulfides have not been observed. Late pyrite occurs as veins and veinlets (Fig. 14A) of up to several 10 cm thick and become gradually more abundant at depth. Late pyrite is commonly associated with small amounts of chalcopyrite, as well as marcasite. Secondary Cu oxides consist of malachite and azurite.

The highest Cu concentrations, obvious by the presence of chalcopyrite and the greenish malachite alterations on the surface, occur in the orebodies (Cs), Baghak, and Dardvey. The Cu values reach up to 0.17 wt.% at Baghak, and the As up to 335 ppm at (Cn). Gold was not detected under the analytic conditions, and Ag values were very low (≤1 ppm). The phosphorous content is also remarkably low (<0.04 wt.%). The sulfur content of the magnetite ore is low in the western calcic skarns (0.1 to 2%), but reaches values of up to 13.7% in the eastern anomalies (for analytic results see Table 11).

## 9. Discussion

### 9.1. Role of the Cenozoic magmatism

Conventional models for skarn mineralization are commonly based on the transport of large volumes of hydrothermal solutions and the

**Table 5**
Representative microprobe analyses of pyroxene from the surface and a drill hole sample of the western calcic skarn (Cs), and from the eastern magnesian skarn at (Cn) (from Boomeri, 1998).

| wt.% | C-south (surface sample) | | | | | C-south (BH-21-8) | | | | |
|---|---|---|---|---|---|---|---|---|---|---|
| $SiO_2$ | 49.49 | 49.49 | 49.19 | 49.15 | 49.7 | 50.01 | 49.77 | 48.92 | 49.63 | 49.42 |
| $Al_2O_3$ | 0.30 | 0.36 | 0.40 | 0.43 | 0.35 | 0.45 | 0.44 | 0.51 | 0.35 | 0.49 |
| $TiO_2$ | – | 0.02 | 0.03 | 0.02 | 0.02 | – | – | 0.02 | 0.01 | 0.05 |
| FeO | 24.00 | 23.16 | 25.82 | 25.16 | 25.16 | 21.44 | 21.49 | 23.98 | 21.62 | 23.77 |
| MnO | 1.19 | 1.01 | 1.29 | 1.01 | 1.01 | 1.10 | 0.98 | 1.20 | 1.05 | 1.03 |
| MgO | 3.01 | 3.68 | 2.01 | 2.37 | 2.37 | 4.38 | 4.41 | 3.05 | 4.33 | 3.08 |
| CaO | 23.2 | 23.56 | 22.85 | 22.65 | 22.65 | 23.21 | 23.22 | 23.10 | 23.26 | 23.04 |
| $Na_2O$ | 0.08 | 0.14 | 0.30 | 0.33 | 0.33 | 0.19 | 0.25 | 0.12 | 0.12 | 0.16 |
| $K_2O$ | 0.05 | 0.05 | 0.02 | 0.10 | 0.10 | 0.03 | 0.02 | 0.01 | – | – |
| Total | 101.36 | 101.47 | 101.92 | 101.25 | 102.22 | 100.80 | 101.02 | 100.91 | 100.37 | 101.03 |
| Numbers of cations on the basis of 6 O | | | | | | | | | | |
| Si | 1.98 | 1.97 | 1.97 | 1.98 | 1.98 | 1.98 | 1.98 | 1.97 | 1.98 | 1.98 |
| Al | 0.01 | 0.02 | 0.02 | 0.02 | 0.02 | 0.02 | 0.02 | 0.02 | 0.02 | 0.02 |
| Ti | – | – | – | – | – | – | – | – | – | – |
| $Fe^{2+}$ | 0.8 | 0.77 | 0.87 | 0.85 | 0.85 | 0.71 | 0.73 | 0.81 | 0.72 | 0.80 |
| Mn | 0.04 | 0.03 | 0.04 | 0.03 | 0.03 | 0.04 | 0.03 | 0.04 | 0.04 | 0.03 |
| Mg | 0.18 | 0.22 | 0.12 | 0.14 | 0.14 | 0.26 | 0.26 | 0.18 | 0.26 | 0.18 |
| Ca | 0.99 | 1.00 | 0.98 | 0.98 | 0.98 | 0.99 | 0.99 | 0.99 | 0.99 | 0.99 |
| Na | 0.01 | 0.01 | 0.02 | 0.03 | 0.03 | 0.01 | 0.02 | 0.01 | 0.01 | 0.01 |
| K | – | – | – | 0.01 | 0.01 | – | – | – | – | – |
| Fe/Al | 80 | 38.5 | 43.5 | 42.5 | 42.5 | 35.5 | 36.5 | 40.5 | 36 | 40 |
| Fe/Ca | 0.81 | 0.77 | 0.89 | 0.87 | 0.87 | 0.72 | 0.74 | 0.82 | 0.73 | 0.81 |
| $(Fe^{2+}+Mg + Mn)$ | 1.02 | 1.02 | 1.03 | 1.02 | 1.02 | 1.01 | 1.02 | 1.03 | 1.02 | 1.01 |
| $X_{Hd}$ | 0.78 | 0.75 | 0.84 | 0.83 | 0.83 | 0.70 | 0.72 | 0.79 | 0.71 | 0.79 |
| $X_{Di}$ | 0.18 | 0.22 | 0.12 | 0.14 | 0.14 | 0.26 | 0.25 | 0.17 | 0.25 | 0.18 |
| $X_{Jo}$ | 0.04 | 0.03 | 0.04 | 0.03 | 0.03 | 0.04 | 0.03 | 0.04 | 0.04 | 0.03 |

| wt.% | Dardvey | | | C-north | | |
|---|---|---|---|---|---|---|
| $SiO_2$ | 53.89 | 55.14 | 51.57 | 53.25 | 53.69 | 54.00 |
| $Al_2O_3$ | 1.63 | 0.52 | 4.12 | 0.03 | – | 0.06 |
| $TiO_2$ | 0.06 | 0.07 | 0.19 | 0.06 | 0.02 | – |
| FeO | 7.47 | 5.21 | 6.02 | 2.23 | 3.30 | 1.48 |
| MnO | 0.27 | 0.88 | 0.21 | 0.10 | 0.10 | 0.09 |
| MgO | 13.76 | 14.79 | 14.02 | 16.91 | 17.24 | 17.00 |
| CaO | 25.31 | 25.49 | 25.76 | 24.89 | 22.77 | 25.16 |
| $Na_2O$ | 0.11 | 0.07 | 0.12 | 0.05 | 0.11 | 0.07 |
| $K_2O$ | 0.02 | – | 0.01 | 0.01 | 0.03 | 0.01 |
| Total | 102.5 | 102.2 | 102.0 | 97.5 | 97.3 | 97.9 |
| Number of cations on the basis of 6 O | | | | | | |
| Si | 1.96 | 2.00 | 1.88 | 1.99 | 1.99 | 1.99 |
| Al | 0.07 | 0.02 | 0.18 | 0.01 | 0.03 | 0.02 |
| Ti | – | – | 0.01 | – | – | – |
| $Fe^{2+}$ | 0.23 | 0.16 | 0.18 | 0.07 | 0.10 | 0.05 |
| Mn | 0.01 | 0.03 | 0.01 | – | – | – |
| Mg | 0.75 | 0.80 | 0.76 | 0.94 | 0.95 | 0.94 |
| Ca | 0.99 | 0.99 | 1.01 | 1.00 | 0.90 | 1.00 |
| Na | 0.01 | – | 0.01 | – | 0.01 | – |
| K | – | – | – | – | – | – |
| Fe/Al | 3.29 | 8.00 | 1.00 | 9.25 | 3.08 | 2.61 |
| Fe/Ca | 0.23 | 0.16 | 0.18 | 0.07 | 0.11 | 0.05 |
| $(Fe^{2+}+Mg + Mn)$ | 0.99 | 0.99 | 0.95 | 1.01 | 1.06 | 0.98 |
| $X_{Hd}$ | 0.23 | 0.16 | 0.19 | 0.07 | 0.10 | 0.05 |
| $X_{Di}$ | 0.76 | 0.81 | 0.80 | 0.93 | 0.90 | 0.95 |
| $X_{Jo}$ | 0.01 | 0.03 | 0.01 | – | – | – |

$X_{Hd} = Fe / (Fe + Mg + Mn)$, $X_{Di} = Mg / (Fe + Mg + Mn)$, $X_{Jo} = Mn / (Fe + Mg + Mn)$; (−) = below detection limit.

presence of reactive lithologies, mainly sedimentary carbonate rocks. The fluids are generally implied to have some magmatic contribution from spatially associated granitic to dioritic intrusions (Bowman et al., 1985, 2008; Brown et al., 1985; Einaudi and Burt, 1982; Einaudi et al., 1981; Kwak, 1987; Layne et al., 1991). At Sangan these plutons consist of quartz alkali syenite porphyry and syenogranite porphyry as part of the larger granitoid series. They crop out close and at the contact of the orebodies and display skarnization at their contact. The age of the ore forming hydrothermal system can be therefore inferred from the intrusion ages, which is 39.1 ± 0.6 Ma to 38.3 ± 0.5 Ma.

The source pluton is part of the Cenozoic magmatism at the active continental margin of the KKB-VPMB of northeastern Iran and displays a high potassium to shoshonitic character with metaluminous to slightly peraluminous affinity. Evidences, such as the magnetite–biotite–hornblende assemblage, the geochemical signature, and the magnetic susceptibility range of the source plutons ($450 \times 10^{-5}$ to $7000 \times 10^{-5}$ SI, Sangan Iron Ore Complex — Iran Eastern Iron Ore Company, IEIOC, 2011) indicate that the granitoids are of I-type. Enrichment in LILE (Cs, Rb, Ba, K, Th, U) and LREE (La, Ce), depletion in HFSE (Nb, Y, Ta, Ti) and HREE (Yb, Lu), and the negative Eu anomalies with low Sr (96 to 362 ppm) contents of the granitoids indicate that subduction played a dominant role in their petrogenesis. The depletion in HFSE with significant negative Nb and Ti anomalies is recognized as a fingerprint of subduction

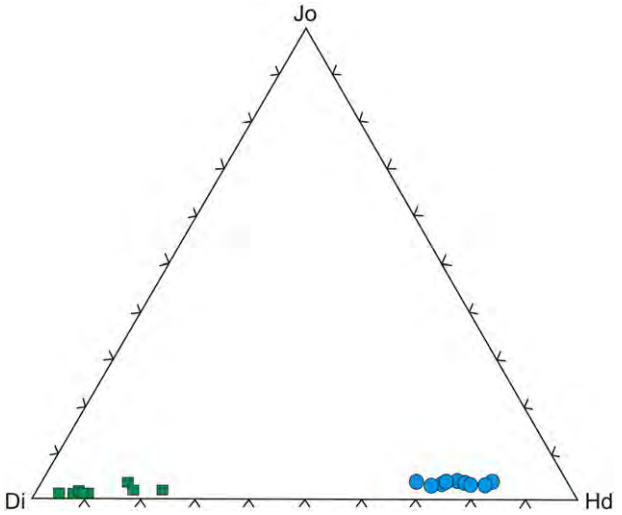


**Fig. 10.** Plot of microprobe analyses of pyroxenes from the western calcic skarn (Anomaly Cs; circles), and eastern magnesian skarn (Anomaly Cn; squares).

processes (e.g., Thirlwall et al., 1994), and suggest that the mantle source has been affected by slab derived components (hydrous fluid or melt). Depletion in HFSE is generally ascribed to the transfer of significant amounts of LILE, but not HFSE, in the slab-derived components. The HFSE are more likely to be sorted in phases such as rutile and/or ilmenite, which may persist in the subducted slab (Ryerson and Watson, 1987). Likewise, the negative Eu anomaly and low Sr contents in Sangan intrusions also indicate that the source magma was plagioclase-bearing. This is due to the very high partition coefficient (D) of Eu ($D_{Eu} = 5.417$) between plagioclase and silicic melt (Nash and Crecraft, 1985). Residual plagioclase would buffer the Sr in the liquid, whereas the partial melt would contain much higher Sr content (Martin et al., 2005), leaving a plagioclase free residue. The studied rocks have also low to moderate $(La/Yb)_N$ of 8.78–32.42, which reflects the presence of plagioclase in the source regions. The negative Eu anomaly therefore, might be explained by the residual plagioclase that was left in the source magma.

### 9.2. Skarn and iron ore formation

Skarn deposits are among the largest iron ores (Meinert, 1992a, 1992b), and with a proven reserve of >1000 Mt high grade iron ore at 53% Fe, the Sangan deposit is one of the largest worldwide. The global iron skarn deposits are compositionally divided into two types, according to the chemistry of their host rocks: (i) calcic skarns and (ii) magnesian skarns. Calcic skarns are associated with iron-rich plutons that are intruded into limestone protoliths, whereas magnesian skarn are associated with diverse plutons in a variety of tectonic settings and they form in dolomitic wallrocks (Meinert, 1992a, 1992b). Calcic skarn minerals are dominated by garnet and pyroxene with less epidote and actinolite, all of which are iron-rich (Purtov et al., 1989). The magnesian skarns mainly consist of forsterite, diopside, phlogopite, serpentine and talc with little iron participating in their mineral composition. This suggests that the available iron in the metasomatic fluid is preferentially incorporated in the magnetite rather than in the structure of andradite or hedenbergite (e.g. Hall et al., 1988). Coexisting calcic and magnesian skarns are reported, among others, from a number of Russian deposits (Aksyu and Zharikov, 1988; Sokolov and Grigor'ev, 1977).

The Sangan deposit is a composite calcic and magnesian type skarn that has been formed due to the presence of two different protoliths consisting of limestone in the west, and dolostone in the east. The chemistry of the skarn minerals reflects the composition of the protolith. The calcic skarn in the west consists of prograde andradite-grossular-rich

**Table 6**
Representative microprobe analyses of amphibole from the western calcic skarns (Á), (A), and (B; this work), and the eastern magnesian skarn at (Cn) (from Boomeri, 1998).

| | Endoskarn | | Exoskarn | | | |
|---|---|---|---|---|---|---|
| wt.% | Anomaly (Á) | | Anomaly (A) | | Anomaly (B) | |
| $SiO_2$ | 38.74 | 38.30 | 48.90 | 48.56 | 48.35 | 48.83 |
| $TiO_2$ | – | 0.12 | 0.03 | 0.03 | – | – |
| $Al_2O_3$ | 9.02 | 9.37 | 1.11 | 1.29 | 1.68 | 1.39 |
| $Cr_2O_3$ | – | – | 0.03 | – | – | – |
| FeO | 31.93 | 31.28 | 31.34 | 31.92 | 30.98 | 30.99 |
| MnO | 0.58 | 0.51 | 0.40 | 0.29 | 0.33 | 0.31 |
| MgO | 2.01 | 2.22 | 3.68 | 3.81 | 4.17 | 4.34 |
| CaO | 11.54 | 11.37 | 11.49 | 11.31 | 11.30 | 11.67 |
| $Na_2O$ | 1.10 | 1.12 | 0.28 | 0.27 | 0.29 | 0.33 |
| $K_2O$ | 2.02 | 2.03 | 0.30 | 0.33 | 0.25 | 0.29 |
| $H_2O$ | – | – | 1.79 | 1.85 | 1.85 | 1.88 |
| F | 0.27 | 0.23 | 0.13 | – | 0.01 | – |
| Cl | 1.72 | 1.77 | 0.15 | 0.15 | 0.13 | 0.09 |
| Total | 100.17 | 99.58 | 99.63 | 99.79 | 99.34 | 100.14 |
| * | 0.10 | 0.11 | 0.17 | 0.18 | 0.19 | 0.20 |
| Numbers of cations on the basis of 24 (O, OH, F, Cl) | | | | | | |
| Si | 6.44 | 6.39 | 7.78 | 7.72 | 7.69 | 7.70 |
| Ti | – | – | – | – | – | – |
| Al | 1.77 | 1.84 | 0.21 | 0.24 | 0.31 | 0.26 |
| Cr | – | – | – | – | – | – |
| $Fe^{2+}$ | 4.44 | 4.37 | 4.17 | 4.24 | 4.12 | 4.09 |
| Mn | 0.08 | 0.07 | 0.05 | 0.04 | 0.04 | 0.04 |
| Mg | 0.50 | 0.55 | 0.87 | 0.90 | 0.99 | 1.02 |
| Ca | 2.06 | 2.03 | 1.96 | 1.93 | 1.93 | 1.97 |
| Na | 0.35 | 0.36 | 0.09 | 0.08 | 0.09 | 0.10 |
| K | 0.43 | 0.43 | 0.06 | 0.07 | 0.05 | 0.06 |

*(Mg)/(Mg + $Fe^{2+}$); (−) = below detection limit/not analyzed

| Samples | C-north | |
|---|---|---|
| $SiO_2$ | 57.09 | 57.39 |
| $Al_2O_3$ | 1.55 | 0.95 |
| $TiO_2$ | 0.04 | 0.01 |
| $Fe_2O_3$[a] | – | – |
| FeO | 5.42 | 8.03 |
| MnO | 0.14 | 0.09 |
| MgO | 20.56 | 19.16 |
| CaO | 12.87 | 12.79 |
| $Na_2O$ | 0.37 | 0.18 |
| $K_2O$ | 0.08 | 0.08 |
| Cl | 0.10 | 0.08 |
| F | 0.31 | 0.16 |
| O | 0.15 | 0.09 |
| $H_2O$[b] | 1.76 | 1.92 |
| Total | 100.13 | 100.76 |
| Numbers of cations on the basis of 23 O | | |
| Si | 7.89 | 7.96 |
| $Al^{IV}$ | 0.11 | 0.04 |
| $Al^{VI}$ | 0.14 | 0.12 |
| Ti | 0.00 | 0.00 |
| $Fe^{3+}$ | 0.00 | 0.00 |
| $Fe^{2+}$ | 0.67 | 0.93 |
| Mn | 0.02 | 0.01 |
| Mg | 4.23 | 3.96 |
| $Fe^{2+}$ | – | – |
| Ca | 1.90 | 1.90 |
| Na | 0.10 | 0.05 |
| K | 0.013 | 0.014 |
| Cl | 0.02 | 0.02 |
| F | 0.13 | 0.07 |
| OH | 1.84 | 1.91 |
| X $Fe^{2+}$ | 0.13 | 0.19 |
| * | 0.87 | 0.81 |

Cations are normalized to sum (Si + Al + Ti + Fe + Mn + Mg + Ca) = 15.
*(Mg) / (Mg + $Fe^{2+}$); (−) = below detection limit.
[a] Calculated from charge balance.
[b] Calculated assuming OH = 2 − (Cl + F).

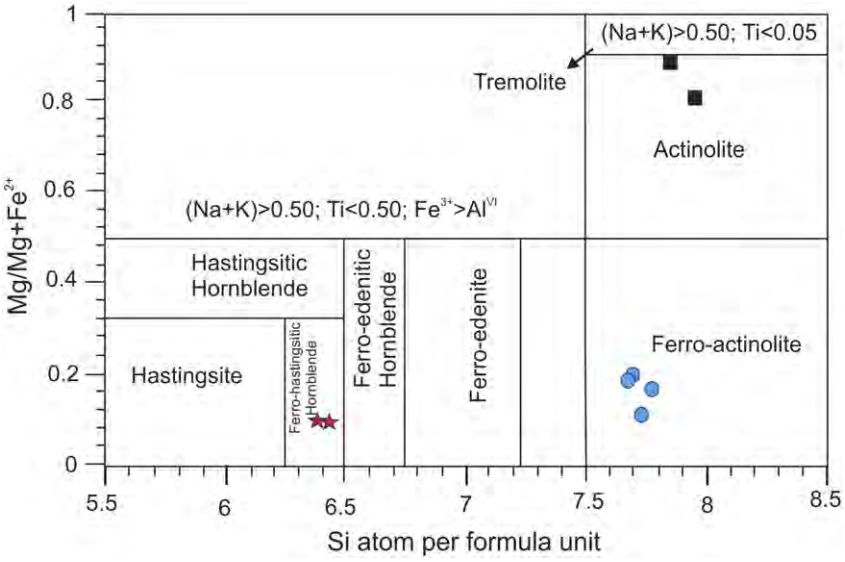


**Fig. 11.** Plot of microprobe analyses showing the compositional range of the amphiboles from the western endoskarn at (Á) (stars) and the exoskarn at (A) and (B) (circles), as well as the eastern exoskarn at (Cn) (squares).
Field boundaries from Leake (1978) and Hawthorne (1985).

garnet, Ca–Fe-rich pyroxene ($Hd_{75.6}Di_{20}Jo_{4.5}$), K–Cl–F-ferrohastingsite that is associated with wollastonite, plagioclase and K-feldspars in the endoskarns, and of retrograde ferroactinolite, Fe-rich chlorite clinochlore, and calcite in the exoskarns. The eastern skarn is magnesian, contains forsterite and diopsidic pyroxene ($Hd_{0.2}Di_{0.88}$,), phlogopite, and retrograde minerals actinolite, serpentine, Mg-chlorite clinochlore, and talc.

Andradite forms according to the following simple reaction at a temperature range between 300 to 520 °C, and at 0.5 kb, and is stable at $XCO_2$ range of 0.1 to 9.6

$$CaCO_3(\text{calcite}) + Fe_2O_3 + 3SiO_2 \rightarrow Ca_3Fe_2Si_3O_{12}(\text{andradite}) + 3CO_2$$

Beyond these conditions, andradite decomposes to magnetite + quartz (Einaudi and Burt, 1982).

A direct relationship exists between the chemistry of the calcsilicate skarn minerals and the type of the associated ore deposit. In this context, andradite garnet is associated with iron mineralization, whereas for example Sn and W ores are considered to be associated with nonferrous, grossular skarns (Einaudi and Burt, 1982). The maximum temperature for the formation of skarn deposits is about 600 °C as summarized by Meinert (1992a, 1992b). Sangan skarns largely consist of andradite with some grossular and minor amounts of pyrope-spessartite ($Adr_{50-83}Grs_{13-45}Sps\text{-}Alm_{3-7}$), which is similar to the global iron skarns. The composition of the pyroxenes associated with the iron skarns is dominated by diopside-hedenbergite, whereas hedenbergite content varies between 20 to 80% (Einaudi et al., 1981; Meinert, 1989). The compositional range of the Sangan pyroxenes is also very close to the values of the common iron skarns. Pyroxene forms at

**Table 7**
Representative microprobe analyses of chlorite from the western calcic skarn (A), and the eastern magnesian skarn Baghak.

| wt.% | Anomaly (A) | | | Baghak | |
|---|---|---|---|---|---|
| $SiO_2$ | 23.58 | 23.71 | 23.30 | 31.85 | 32.04 |
| $TiO_2$ | 0.03 | 0.01 | 0.02 | 0.05 | 0.04 |
| $Al_2O_3$ | 18.62 | 18.68 | 18.76 | 17.88 | 18.62 |
| FeO | 40.59 | 40.09 | 39.63 | 1.93 | 1.76 |
| MnO | 0.16 | 0.08 | 0.15 | 0.02 | 0.04 |
| MgO | 5.42 | 6.08 | 5.96 | 35.34 | 33.85 |
| CaO | 0.94 | 0.09 | 0.13 | 0.05 | 0.17 |
| $Na_2O$ | – | – | – | 0.02 | – |
| $K_2O$ | – | – | – | 0.03 | 1.20 |
| $H_2O$ | 10.57 | 10.55 | 10.46 | 11.61 | 11.69 |
| Total | 99.91 | 99.29 | 98.41 | 98.78 | 99.41 |
| Si | 5.35 | 5.39 | 5.34 | 5.95 | 5.98 |
| $Al^{(4)}$ | 2.65 | 2.61 | 2.66 | 2.05 | 2.02 |
| Total | 8.00 | 8.00 | 8.00 | 8.00 | 8.00 |
| $Al^{(6)}$ | 2.33 | 2.39 | 2.41 | 1.89 | 2.08 |
| Ti | 0.01 | – | – | 0.01 | 0.01 |
| $Fe^{3+}$ | 7.70 | 7.62 | 7.60 | 0.30 | 0.27 |
| Mn | 0.03 | 0.02 | 0.03 | – | 0.01 |
| Mg | 1.83 | 2.06 | 2.04 | 9.85 | 9.42 |
| Ca | 0.23 | 0.02 | 0.03 | 0.01 | 0.03 |
| Na | – | – | – | 0.01 | – |
| K | – | – | – | 0.01 | 0.29 |
| Total | 12.15 | 12.11 | 12.12 | 12.08 | 12.11 |
| Total | 20.15 | 20.11 | 20.12 | 20.08 | 20.11 |
| Si p.f.u. | 5.35 | 5.39 | 5.34 | 5.95 | 5.98 |
| * | 0.81 | 0.79 | 0.79 | 0.03 | 0.03 |

*(Fe + Mn) / (Fe + Mn + Mg); (−) = below detection limit.

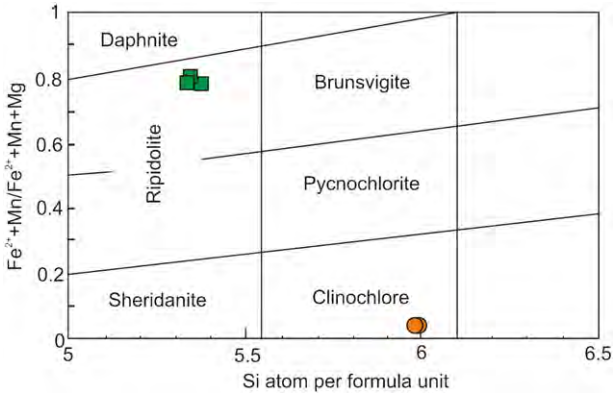


**Fig. 12.** Plot of microprobe analyses showing the compositional range of chlorites from the western calcic skarn (A; squares), and the eastern magnesian skarn Baghak (circles).

**Table 8**
Representative microprobe analyses of forsterite from the eastern magnesian skarn (Cn).

| wt.% | C-north | | |
|---|---|---|---|
| $SiO_2$ | 41.60 | 41.12 | 40.88 |
| $TiO_2$ | – | – | – |
| $Al_2O_3$ | – | – | – |
| $Cr_2O_3$ | – | – | – |
| FeO | 2.75 | 2.96 | 2.82 |
| MnO | 0.77 | 0.56 | 0.68 |
| NiO | – | 0.06 | – |
| MgO | 55.72 | 56.05 | 54.91 |
| CaO | 0.03 | 0.02 | 0.05 |
| $Na_2O$ | – | 0.03 | – |
| $K_2O$ | – | – | – |
| $P_2O_5$ | – | – | – |
| $SO_3$ | 0.14 | 0.06 | – |
| Cl | – | – | – |
| Total | 101.04 | 100.89 | 99.37 |
| * | 0.03 | 0.03 | 0.03 |
| Numbers of cations on the basis of 24 (O, Cl) | | | |
| Si | 5.88 | 5.83 | 5.88 |
| Ti | – | – | – |
| Al | – | – | – |
| Cr | – | – | – |
| $Fe^{2+}$ | 0.33 | 0.35 | 0.34 |
| Mn | 0.09 | 0.07 | 0.08 |
| Ni | – | – | – |
| Mg | 11.75 | 11.86 | 11.77 |
| Ca | – | – | – |
| Na | – | – | – |
| K | – | – | – |
| P | – | – | – |
| S | 0.02 | – | – |

$(Fe^{2+}+Mn)$ / $(Fe^{2+}+Mn + Mg)$; (−) = below detection limit.

temperatures above 520 °C, 2 kb and $XCO_2$ <0.7 (Einaudi et al. (1981)), and is commonly converted to amphibole beyond these conditions. This retrograde reaction is commonly observed at Sangan, where amphibole widely occurs as large, fibrous crystals and crystal aggregates of ferroactinolite in particular in the western anomalies (A), (Á), (B), and (Cs). The presence of F–Cl–K-hastingsite together with pyroxene in the western calcic endoskarns indicate a high temperature prograde metasomatism, whereas the ferroactinolite-calcite-ferrochlorite association indicates a retrograde alteration. Based on the intimate spatial relationships between the calcsilicate skarns and the source plutons, and the presence of high temperature garnet-pyroxene mineral assemblage, the estimated temperatures at the endoskarn (Á) and at Dardvey should have been above 400 °C. Depending on their chemical composition, the stability temperature of the chlorites at Sangan has been calculated between 259 and 310 °C (Karimpour, 1999). The presence of K-bearing hastingsite in the calcic skarn and the phlogopite in the magnesian skarn suggests that the skarn fluids were K-rich. The mineralization at Sangan is magnetite-rich and is associated with minor amounts of sulfides that consist of pyrrhotite, chalcopyrite and pyrite. The higher MgO contents of the calcsilicate minerals and the magnetite in the eastern magnesian skarns (3.65 wt.% MgO), and less than 0.2 wt.% MgO in the calcic skarns reflects the composition of their protoliths.

The formation of the Sangan iron skarn deposit along the northern margin of the major Doruneh Fault is related to the tectonomagmatic evolution of the KKB-VPMB, and the ore fluids appear to have been conducted along this major fault zone to the shallower depositional levels. The observation that high temperature contact skarn minerals garnet and pyroxene actually occur on the surface outcrops at the contact with the source pluton at Anomaly (Á) and at Dardvay areas on the subsurface, indicates a deep erosional level, whereas the presence of low temperature mineral assemblages and lake of the source intrusions in other parts of the deposit mark the shallow formational levels as shown schematically in Fig. 15.

## 10. Conclusions

The worldclass Sangan iron ore deposit formed due to the intrusion of granitoid bodies of quartz alkali syenite to quartz syenite and syenogranite composition into the Cretaceous carbonate rocks. The source granitoid pluton is calcalkaline, metaluminous to slightly peraluminous, and of I-type. They show trace element features typical of the magmatism related to the subduction zones with a possible depleted mantle input. The whole process took place as a result of the Cenozoic magmatism along the Khaf-Kashmar-Bardaskan Volcano-Plutonic-Metallogenic Belt of northeastern Iran. The age of the source pluton is Middle Eocene (39.1 ± 0.6 to 38.3 ± 0.5 Ma). The very high tonnage of the iron ore formed at Sangan indicates large scale transfer of huge masses of iron-bearing brines from an iron-rich source magma within the KKB-VPMB. The ore brines were possibly transferred along the major E–W structure of Doruneh Fault to the shallower depositional levels.

The intimate association of the skarns with the iron orebodies, the common mineral paragenetic associations, as well as the mineral chemistry at Sangan indicates a common metasomatic-hydrothermal system for both the iron ore and the calcsilicate skarns, whereas the calcsilicate skarns have been overprinted by the iron ore. The skarn mineralogy is represented by high temperature mineral assemblages, and district variation in the skarn mineralogy at Sangan reflects local differences in the composition of the host protoliths that is calcic in the west and magnesian in the east. The western skarn consists of Ca-rich calcsilicates, whereas the calcsilicates, as well as the magnetite ore in the eastern dolostone host are Mg-rich. The presence of K-bearing hastingsite in the calcic skarn and phlogopite in the magnesian skarn indicate K-rich metasomatic fluids. This view is reinforced by the high-K to shoshonitic nature of the source fluids.

## Acknowledgments

We would like to thank Sangan Iron Ore Complex for the generous support and the access to the mine data. Our thanks go to the Colorado School of Mines for the use of the EMP, and to Dr. G. Gehrels and Dr. V. Valencia (University of Arizona) for the U–Pb zircon dating, and to Professor L. Fontboté (University of Genève) for the constructive review of the manuscript. Extensive revision accompanied by a field visit and microscopic work by Dr. F. Daliran (Karlsruhe Institute of Technology, Germany), as well as her editorial work is greatly appreciated.

## References

Aghanabati, A., 2004. Geology of Iran. Geological Survey of Iran, Report No. 35 (230 pp.).
Aksyu, A.M., Zharikov, V.A., 1988. The phlogopite skarn deposits: physical–chemical conditions of formation. In: Zachrisson, E. (Ed.), Proceeding of the 7th Quadrennial IAGOD Symposium. Schweizerbart, Stuttgart, pp. 321–326.
Boomeri, M., 1998. Petrography and geochemistry of the Sangan iron skarn deposit and related igneous rocks, northeastern Iran(PhD Thesis) Akita University, Japan (226 pp.).
Bowman, J.R., O'Neil, J.R., Essene, E.J., 1985. Contact skarn formation at Elkhorn, Montana: II. Origin and evolution of C–O–H skarn fluids. Am. J. Sci. 283, 621–660.
Bowman, J.R., Covert, J.J., Clark, A.H., Mathieson, G.A., 2008. The GanTung E zone scheelite skarn orebody, tungsten, Northwest Territories; oxygen, hydrogen and carbon isotope studies. Econ. Geol. 80, 1872–1895.
Boynton, W.V., 1984. Cosmochemistry of the rare earth elements: meteorite studies. In: Henderson, P. (Ed.), Rare Earth Element Geochemistry.
Brown, P.E., Bowman, J.R., Kelly, W.C., 1985. Petrologic and stable isotope constraints on source and evolution of skarn-forming fluids at Pine Creek, California. Econ. Geol. 80, 72–95.
Chapell, B., White, A., 2001. Two contrasting granite types: 25 years later. Aust. J. Earth Sci. 48, 489–499.
Cherniak, D.J., Watson, E.B., 2000. Pb diffusion in zircon. Chem. Geol. 172, 5–24.
Eftekharnejad, J., 1981. Tectonic division of Iran with respect to sedimentary basins. J Iran Petrol Soc 82, 19–28 (in Persian).
Einaudi, M.T., Burt, D.M., 1982. Introduction — terminology, classification and composition of skarn deposits. Econ. Geol. 77, 745–754.
Einaudi, M.T., Meinert, L.D., Newberry, R.J., 1981. Skarn deposits. Economic Geology 75th Anniversary Volume, pp. 317–391.

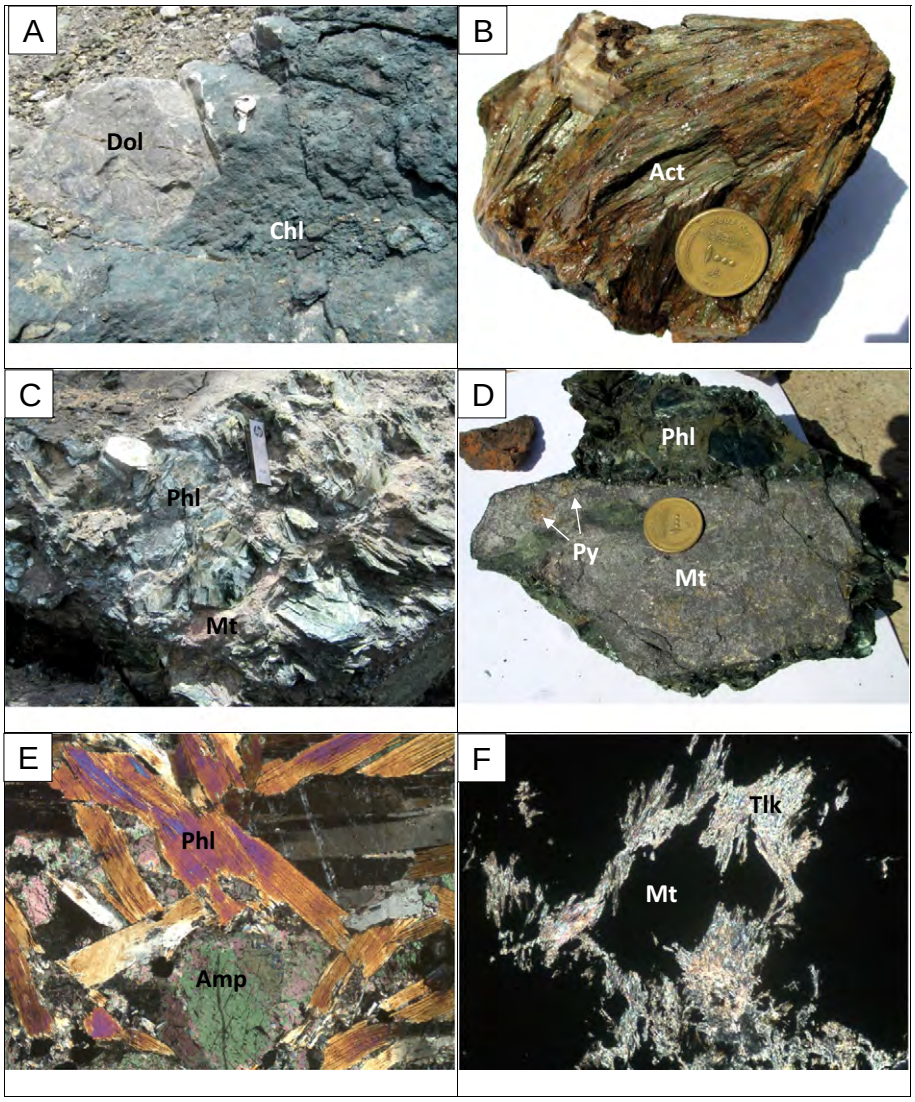


**Fig. 13.** Field, hand specimen, and microphotographs from the eastern magnesian skarn at Baghak showing A) Skarnization with retrograde Mg-rich chlorite at the contact of the recrystallized dolomites; B) large, pale green crystal aggregates of actinolite, Baghak Anomaly; C) large sheets of phlogopite associated with the magnetite ore; D) close view of (C) showing large sheets of the dark green phlogopite. Magnetite is spotted with late pyrite-chalcopyrite; D) large sheets of phlogopite associated with amphibole; E) Talc alteration. Act: actinolite; Amp: amphibole; Chl: chlorite; Cpy: chalcopyrite; Dol: dolomite; Mt: magnetite; Phl: phlogopite; Py: pyrite; Tlk: talk. Width of both microphotographs is 1.2 mm.

Gehrels, G.E., Valencia, V.A., Ruiz, J., 2008. Enhanced precision, accuracy, efficiency, and spatial resolution of U–Pb ages by laser ablation-multicollector-inductively coupled plasma-mass spectrometry. Geochem. Geophys. Geosyst. 9, 13.
Gill, J.B., 1981. Orogenic Andesites and Plate Tectonics. Springer, Berlin (390 pp.).
Gust, D.A., Arculus, R.A., Kersting, A.B., 1997. Aspects of magma sources and processes in the Honshu arc. Can. Mineral. 35, 347–365.
Hall, D.L., Cohen, L.H., Schiffman, P., 1988. Hydrothermal alteration associated with the Iron Hat iron skarn deposit, eastern Mojave Desert, San Bernardino County, California. Econ. Geol. 83, 568–587.
Hawthorne, F.C., 1985. Crystal chemistry of the amphiboles. Rev. Mineral. 9A, 1–102.
Irvine, T., Baragar, W., 1971. A guide to the chemical classification of the common volcanic rocks. Can. J. Earth Sci. 8, 523–548.
Karimpour, M.H., 1999. Temperature, formation, and magnetite paragenesis in different places of Sangan iron mine. Proceedings of 17th Earth Sciences Conference, Tehran, pp. 161–167.
Karimpour, M.H., 2004. Mineralogy, alteration, source rock, and tectonic setting of iron-oxides Cu–Au deposits and examples of Iran. 11th Iranian Crystallography and Mineralogy Society of Iran Conference. University of Yazad, pp. 184–189.
Karimpour, M.H., Malekzadeh Shafaroudi, A., 2006. Comparison of the geochemistry of source rocks at Tanbnurjeh Au-bearing magnetite and Sangan Au-free magnetite deposits, Khorasan Razavi, Iran. Iran. J. Crystallogr. Mineral. 13 (1), 3–26.
Karimpour, M.H., Malekzadeh Shafaroudi, A., 2008. Skarn geochemistry — mineralogy and petrology of source rock, Sangan Iron mine, Khorasan Razavi, Iran. Sci. Q. J. Geosci. 65, 108–125.
Kwak, T.A.P., 1987. W–Sn skarn deposits and related metamorphic skarns and granitoids. Development in Economic Geology. , 24. Elsevier, Amsterdam, p. 468.
Layne, G.D., Longstaffe, F.J., Spooner, E.T.C., 1991. The JC tin skarn deposit, southern Yukon Territory: II. A carbon, oxygen, hydrogen, and sulfur stable isotope study. Econ. Geol. 86, 48–65.
Leake, B.E., 1978. Nomenclature of amphiboles. Am. Mineral. 63, 1023–1052.
Malekzadeh Shafaroudi, A., Karimpour, M.H., Golmohammadi, A., 2013. Zircon U–Pb geochronology and petrology of intrusive rocks in the C-North and Baghak districts, Sangan iron mine, NE Iran. J. Asian Earth Sci. 64, 256–271.
Maniar, P.D., Piccoli, P.M., 1989. Tectonic discrimination of granitoids. Geol. Soc. Am. Bull. 101, 635–643.
Martin, H., 1999. The adakitic magmas: modern analogues of Archaean granitoids. Lithos 46, 411–429.
Martin, H., Smithies, R.H., Rapp, R., Moyen, J.F., Champion, D., 2005. An overview of adakite, tonalite-trondhjemite-granodiorite (TTG), and sanukitoid: relationships and some implications for crustal evolution. Lithos 79, 1–24.
Mazloomi, A., Karimpour, M.H., Rasa, I., Rahimi, B., Vosoghi Abedini, M., 2009. Kuh-e-Zar gold deposit of Torbat-e-Hydarieh: new model of gold mineralization. Iran. J. Crystallogr. Mineral. 16, 364–376 (in Persian with English abstract).

**Table 9**
Representative microprobe analyses of phlogopite from the eastern skarns (Cn), Baghak, and Dardvay.

| wt. % | C-north | Baghak | | | Dardvey | |
|---|---|---|---|---|---|---|
| $SiO_2$ | 39.78 | 43.62 | 39.17 | 39.45 | 40.65 | 40.15 |
| $TiO_2$ | 0.05 | 0.09 | 0.21 | 0.25 | – | 0.05 |
| $Al_2O_3$ | 12.20 | 11.18 | 15.86 | 15.40 | 14.85 | 14.99 |
| FeO | 1.90 | 5.50 | 3.97 | 2.54 | 2.24 | 2.60 |
| MnO | 0.04 | 0.02 | 0.04 | 0.15 | 0.08 | – |
| MgO | 26.13 | 25.01 | 24.85 | 25.53 | 25.61 | 25.66 |
| CaO | – | – | 0.02 | 0.03 | – | – |
| $Na_2O$ | 0.16 | 0.14 | 0.14 | 0.17 | 0.13 | 0.14 |
| $K_2O$ | 10.68 | 9.21 | 10.32 | 10.58 | 10.72 | 10.71 |
| $H_2O$ | 3.60 | 3.27 | 3.44 | 3.32 | 3.14 | 3.01 |
| F | 1.25 | 1.87 | 1.59 | 1.82 | 2.22 | 2.50 |
| Cl | 0.02 | 0.27 | 0.01 | 0.03 | 0.08 | 0.04 |
| Total | 98.82 | 100.19 | 99.64 | 99.28 | 99.73 | 99.84 |
| * | 0.04 | 0.11 | 0.08 | 0.06 | 0.04 | 0.05 |
| Numbers of cations on the basis of 24 (O, OH, F, Cl) | | | | | | |
| Si | 5.68 | 6.18 | 5.60 | 5.64 | 5.78 | 5.73 |
| Ti | – | 0.01 | 0.02 | 0.03 | – | – |
| Al | 2.56 | 1.87 | 2.67 | 2.60 | 2.49 | 2.52 |
| $Fe^{2+}$ | 0.23 | 0.65 | 0.48 | 0.30 | 0.27 | 0.31 |
| Mn | – | – | – | 0.02 | – | – |
| Mg | 5.56 | 5.29 | 5.30 | 5.44 | 5.43 | 5.45 |
| Ca | – | – | – | – | – | – |
| Na | 0.04 | 0.04 | 0.04 | 0.05 | 0.04 | 0.04 |
| K | 1.95 | 1.67 | 1.88 | 1.93 | 1.95 | 1.95 |

$(Fe^{2+}+Mn)$ / $(Fe^{2+}+Mn + Mg)$; (−) = below detection limit.


Meinert, L.D., 1989. Gold skarn deposits - Geology and exploration criteria. In: Groves, D., Keays, R., Ramsay, R. (Eds.), Proc. of Gold '88, Economic Geology Monograph #6, pp. 537–552.

Meinert, L.D., 1992a. Skarns and skarn deposits. Geosci. Can. 19, 145–162.

Meinert, L.D., 1992b. Skarn zonation and fluid evolution in the Groundhog Mine, Central Mining District, New Mexico. Econ. Geol. 82, 523–545.

Meinert, L.D., 1995. Compositional variation of igneous rocks associated with skarn deposits — chemical evidence for a genetic connection between petrogenesis and mineralization. Mineral. Assoc. Can. Short Course Ser. 23, 401–418.

Middlemost, E.A.K., 1994. Naming materials in the magma/igneous rock system. Earth-Sci. Rev. 37, 215–224.

Mostowfi Ghazvini, H. (1339) Nuzhat al-qulub.

Nash, W.P., Crecraft, H.R., 1985. Partition coefficients for trace elements in silicic magmas. Geochim. Cosmochim. Acta 49, 2309–2322.

Pearce, J.A., 1983. Role of the sub-continental lithosphere in magma genesis at active continental margins. In: Hawkesworth, C.J., Norry, M.J. (Eds.), Continental Basalts and Mantle Xenoliths. Shiva, Nantwich, pp. 230–249.

Pearce, J.A., Parkinson, I.J., 1993. Trace element models for mantle melting: application to volcanic arc petrogenesis. In: Prichard, H.M., Albaster, T., Harris, N.B.W., Neary, C.R. (Eds.), Magmatic Processes in Plate Tectonics. Geological Society of London Special Publication, 76, pp. 373–403.

Purtov, V.K., Kholodnoc, V.V., Anfilogov, V.N., Nechkin, G.S., 1989. The role of chlorine in the formation of magnetite skarn. Int. Geol. Rev. 31, 63–71.

Reagan, M.K., Gill, J.B., 1989. Coexisting calc-alkaline and high niobium basalts from Turrialba volcano, Costa Rica: implication for residual titanates in arc magma source. J. Geophys. Res. 94, 4619–4633.

Ryerson, F.J., Watson, E.B., 1987. Rutile saturation in magmas: implications for Ti–Nb–Ta depletion in island-arc basalts. Earth Planet. Sci. Lett. 86, 225–239.

Sangan Iron Ore Complex — Iran Eastern Iron Ore Company (IEIOC), 2011. Magnetometric anomalies at Sangan Mine, Baghak and (Cn). IEIOC Internal Mine Report (171 pp.).

Sokolov, G.A., Grigor'ev, V.M., 1977. Deposits of iron. In: Smirnov, V.I. (Ed.), Ore Deposits of the USS 1. Pittman, London, pp. 7–113.

Sun, S.S., McDonough, W.F., 1989. Chemical and isotopy systematics of oceanic basalts: implications for mantle composition and processes. In: Saunders, A.D., Norry, M.J. (Eds.), Magmatism in the Ocean: Basins. The Geological Society of London, Special Publication, 42, pp. 313–345.

Thirlwall, M.F., Smith, T.E., Graham, A.M., Theodorou, N., Hollings, P., Davidson, J.P., Arculus, R.J., 1994. High field strength element anomalies in arc lavas: source or process? J. Petrol. 35, 819–838.

Walker, J.A., Patino, L.C., Carr, M.J., Feigenson, M.D., 2001. Slab control over HFSE depletions in central Nicaragua. Earth Planet. Sci. Lett. 192, 533–543.

Wilson, M., 1989. Igneous Petrogenesis: A Global Tectonic Approach. Harper Collins Academic (466 pp.).

Woodhead, J., Eggins, S., Gamble, J., 1993. High field strength and transition element systematics in island arc and back-arc basin basalts: evidence for multi-phase melt extraction and a depleted mantle wedge. Earth Planet. Sci. Lett. 114, 491–504.

Yousefi, L., Karimpour, M.H., Hidarian Shahri, M.R., 2009. Geology, mineralogy, fluid inclusion microthermometry, and ground magnetic survey of magnetite-specularite copper–gold mineralization of Shaharak prospect area, Torbat-e-Hydarieh, Iran. Iran. J. Crystallogr. Mineral. 16, 505–516 (in Persian with English abstract).

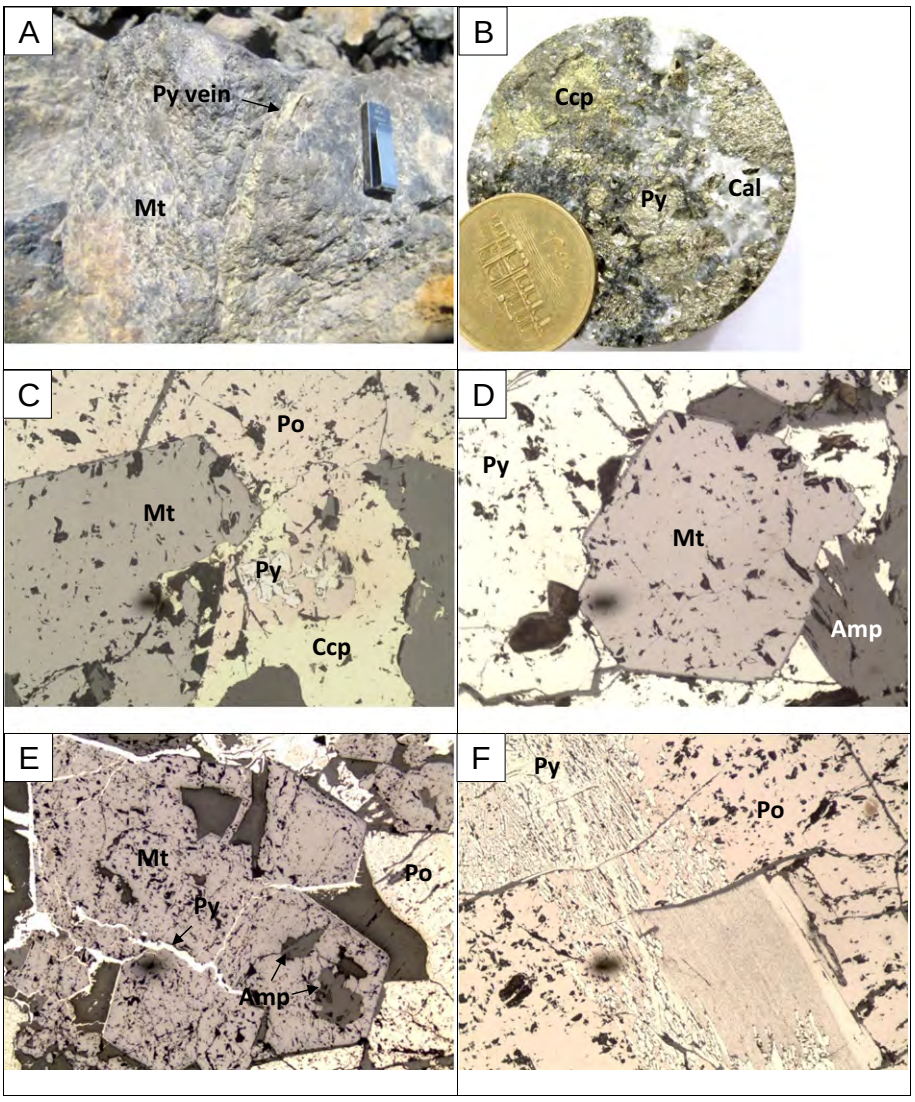


**Fig. 14.** Field, hand specimen, and microphotographs of the magnetite-rich ore at Sangan. A) Massive magnetite ore crosscut by a thin vein of late pyrite, Baghak Anomaly; B) chalcopyrite-pyrite crosscut by late calcite veins, C-south Anomaly (BH 69, 310 m); C, D, E, F) idiomorphic magnetite grains associated with sulfide minerals pyrrhotite, chalcopyrite and pyrite. Note partial replacement of pyrrhotite by semi-oriented, network-like pyrite aggregates. Amp: amphibole; Cal: calcite; Ccp: chalcopyrite; Mt: magnetite; Po: pyrrhotite; Py: pyrite. Width of microphotographs (C), (D), (F) is 1.2 mm, and 4.8 mm for (E).

**Table 10**
Representative microprobe analyses of magnetite from the western and the eastern Sangan orebodies.

| | Western orebodies | | | | | | | | | Eastern orebodies | | | | | | | | | | | |
|---|---|---|---|---|---|---|---|---|---|---|---|---|---|---|---|---|---|---|---|---|---|
| wt.% | Anomaly (Á) | | | | | | Anomaly (B) | | | Baghak | | | | | | C-north | | | Dardvey | | |
| $Fe_2O_3$ | 68.75 | 69.06 | 68.19 | 68.12 | 67.24 | 68.55 | 66.49 | 67.68 | 67.18 | 68.28 | 68.84 | 69.04 | 68.83 | 69.60 | 70.56 | 69.47 | 68.98 | 69.58 | 68.09 | 69.48 | 68.22 |
| FeO | 30.84 | 30.97 | 30.50 | 30.52 | 29.84 | 30.38 | 29.86 | 30.13 | 30.09 | 30.34 | 29.2 | 29.00 | 29.01 | 25.60 | 24.99 | 27.09 | 27.20 | 27.00 | 28.14 | 28.74 | 30.67 |
| $TiO_2$ | – | 0.02 | 0.03 | – | 0.06 | 0.03 | 0.03 | – | – | 0.14 | 0.12 | 0.03 | 0.04 | 0.03 | – | 0.09 | – | 0.01 | 0.03 | – | 0.05 |
| MgO | 0.04 | 0.02 | 0.03 | 0.02 | 0.22 | 0.23 | 0.01 | 0.18 | 0.04 | 0.25 | 1.11 | 1.14 | 1.10 | 3.14 | 3.65 | 2.39 | 2.14 | 2.31 | 1.22 | 1.26 | 0.03 |
| CaO | 0.02 | – | – | – | 0.06 | 0.04 | – | – | 0.11 | – | 0.02 | 0.05 | 0.09 | – | 0.02 | 0.01 | – | – | – | – | 0.03 |
| MnO | 0.03 | 0.12 | 0.14 | 0.10 | 0.12 | 0.09 | 0.08 | 0.02 | 0.07 | 0.20 | – | 0.11 | 0.06 | 0.18 | 0.24 | 0.05 | 0.03 | 0.20 | 0.36 | 0.28 | 0.11 |
| NiO | | – | – | 0.02 | – | 0.06 | 0.07 | – | – | – | – | – | – | 0.03 | 0.06 | – | – | – | – | 0.01 | 0.04 |
| $Cr_2O_3$ | 0.02 | 0.03 | – | 0.02 | 0.01 | – | 0.02 | 0.02 | – | – | 0.03 | 0.02 | – | 0.02 | 0.02 | – | 0.02 | – | – | 0.01 | 0.01 |
| Total | 99.75 | 99.89 | 99.84 | 99.8 | 98.66 | 98.6 | 99.94 | 98.95 | 99.79 | 98.57 | 93.63 | 93.40 | 93.65 | 82.13 | 79.50 | 86.42 | 87.65 | 86.86 | 92.78 | 92.78 | 99.83 |

**Table 11**
Ore reserves and bulk analysis of the magnetite ore samples of the Sangan orebodies.

| Ore body | (Á) | | | (A) | | | (B) | | | C–south |
|---|---|---|---|---|---|---|---|---|---|---|
| Reserve (t) | 39 | | | 173 | | | 235 | | | 157 |
| Hole no. | TP44 | TP34 | TP44 | AK30 | AK49 | AK16 | BH49 | BH003A | BH017 | CSK10 |
| Coordination | 60°24′56″ 34°29′20″ | 60°24′58″ 34°29′19″ | 60°24′56″ 34°29′20″ | 60°25′34″ 34°28′45′ | 60°25′18″ 34°28′52″ | 60°25′35″ 34°28′43″ | 60°26′11″ 34°28′36″ | 60°26′19″ 34°28′32″ | 60°26′01″ 34°28′42″ | 60°25′17″ 34°28′50″ |
| Depth (m) | 43.60–45.60 | 40.30–43.30 | 69.80–72.80 | 55.90–58.80 | 30.40–33.80 | 126.5–129.5 | 322.7–326.7 | 341–346 | 257.5–262.5 | 141–144 |
| Sample no. | TP237 | TP238 | TP239 | SAA240 | SAA241 | SAA242 | SAB255 | SAB256 | SAB257 | SACS43 |
| Fe (wt.%) | 56.70 | 59.90 | 56.90 | 42.80 | 57.00 | 60.30 | 56.50 | 48.51 | 50.89 | 53.20 |
| P | 0.03 | 0.21 | – | – | – | – | – | 0.04 | 0.02 | – |
| S | – | – | 2.04 | 1.11 | 0.24 | 0.09 | 0.04 | 0.19 | 0.04 | 0.15 |
| Cu (ppm) | 24 | 28 | 337 | 162 | 24 | 14 | – | – | – | 9 |
| Pb | 5 | 4 | 3 | 7 | 8 | 6 | – | – | – | 6 |
| Zn | 20 | 25 | 28 | 25 | 49 | 12 | – | – | – | 13 |
| Au | <0.1 | <0.1 | <0.1 | <0.1 | <0.1 | <0.1 | – | – | – | <0.1 |
| As | 5 | 10 | 18 | 43 | 12 | 8 | – | – | – | 13 |
| Co | 11 | 15 | 34 | 31 | 14 | 6 | – | – | – | 3 |
| Ni | 8 | 10 | 22 | 28 | 17 | 15 | – | – | – | 5 |
| Mn | 901 | 727 | 1263 | 2275 | 650 | 899 | – | – | – | 242 |
| Ag (ppb) | 125 | 46 | 115 | 183 | 71 | 57 | – | – | – | 41 |

| Ore body | C–south | | C-north | | | Baghak | | | Dardvey | | |
|---|---|---|---|---|---|---|---|---|---|---|---|
| Reserve (t) | 157 | | 104 | | | 185 | | | 139 | | |
| Hole no. | CSK4 | CSK12 | BH45 | BH86 | BH92 | BK22 | BK22 | BK82 | D87 | D76 | D118 |
| Coordination | 60°26′44″ 34°28′40″ | 60°25′32″ 34°28′45″ | 60°27′14″ 34°28′55″ | 60°27′06″ 34°29′04″ | 60°27′18″ 34°29′04″ | 60°28′17″ 34°28′41″ | 60°28′17″ 34°28′41″ | 60°28′22″ 34°28′41″ | 60°28′12″ 34°29′20″ | 60°28′08″ 34°29′20″ | 60°28′26″ 34°29′12″ |
| Depth (m) | 307–310 | 104.8–107.8 | 70.6–73.8 | 291.3–295.3 | 248.4–252.4 | 101–104 | 222–225 | 244.5–249.5 | 37–40 | 97–100 | 123–126 |
| Sample no. | SACS44 | SACS45 | SACN252 | SACN253 | SACN254 | SABA246 | SABA247 | SABA248 | SAD249 | SAD250 | SAD251 |
| Fe (wt.%) | 57.10 | 41.80 | 57.40 | 54.50 | 58.50 | 46.20 | 52.10 | 50.80 | 60.30 | 61.20 | 46.00 |
| P | – | – | 0.02 | 0.03 | 0.03 | – | – | – | – | – | – |
| S | 0.13 | 5.12 | 0.54 | 2.57 | 2.77 | 0.02 | 13.70 | 0.88 | 0.01 | 1.85 | 0.02 |
| Cu (ppm) | 12 | 571 | – | – | – | 117 | 1667 | 59 | 10 | 827 | 8 |
| Pb | 4 | 2 | – | – | – | 5 | 163 | 6 | 6 | 4 | 4 |
| Zn | 25 | 9 | – | – | – | 57 | 265 | 140 | 81 | 124 | 14 |
| Au | <0.1 | <0.1 | – | – | – | <0.1 | <0.1 | <0.1 | <0.1 | <0.1 | <0.1 |
| As | 7 | 335 | – | – | – | 45 | 168 | 42 | 6 | 33 | 7 |
| Co | 2 | 65 | – | – | – | 30 | 233 | 36 | 13 | 102 | 9 |
| Ni | 6 | 261 | – | – | – | 4 | 59 | 10 | 13 | 33 | 8 |
| Mn | 814 | 1343 | – | – | – | 2215 | 974 | 797 | 925 | 610 | 836 |
| Ag (ppb) | 58 | 283 | – | – | – | 61 | 1042 | 87 | 67 | 291 | 60 |

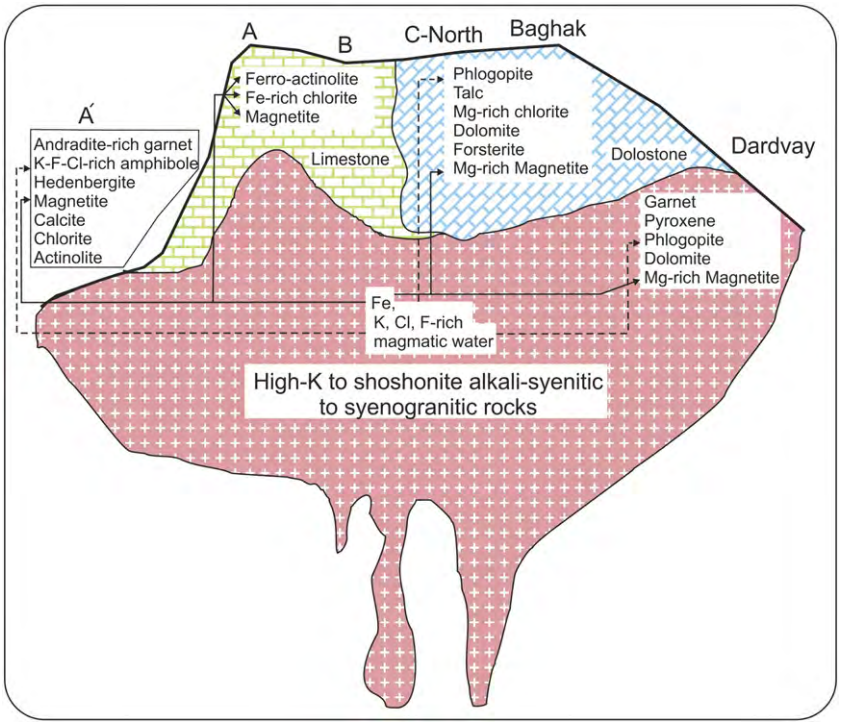


**Fig. 15.** Schematic model showing the spatial relationship between the calcic and magnesian skarn types and the source pluton at Sangan iron skarn ore (not to scale).